Oxidovanadium(V) coordination compounds based on 1,5-bis(2-hydroxy-3-methoxybenzylidene)carbohydrazide: from discrete to polymeric assemblies

*Diana Dragancea, *[a] Natalia Talmaci, [b] Sergiu Shova, [c] Anamaria Hanganu, [a]*

*Simon Grabowsky, [d] Silvio Decurtins, [e] Shi-Xia Liu [e] and Svetlana G. Baca *[f]*

[a] "C. D. Nenitzescu" Institute of Organic and Supramolecular Chemistry of the Romanian Academy, Splaiul Independentei 202B, Bucharest, Romania

[b] Institute of Chemistry, Moldova State University, Academy str., 3, MD2028, Chisinau, Republic of Moldova

[c] "Petru Poni" Institute of Macromolecular Chemistry of the Romanian Academy, Aleea Grigore Ghica Vodă 41-A, RO-700487 Iasi, Romania.

[d] Department of Chemistry, Biochemistry & Pharmaceutical Sciences, University of Bern, Freiestrasse 3, CH-3012 Bern, Switzerland

[e] Department of Chemistry, Biochemistry & Pharmaceutical Sciences, W. Inäbnit Laboratory for Molecular Quantum Materials and WSS-Research Center for Molecular Quantum Systems, University of Bern, Freiestrasse 3, CH-3012 Bern, Switzerland

[f] Institute of Applied Physics, Moldova State University, Academy str., 5, MD2028, Chisinau, Republic of Moldova

Corresponding authors:

* D.D. E-mail: ddragancea@gmail.com

* S.G.B. E-mail: svetlana.baca@ifa.usm.md; sbaca_md@yahoo.com

Content

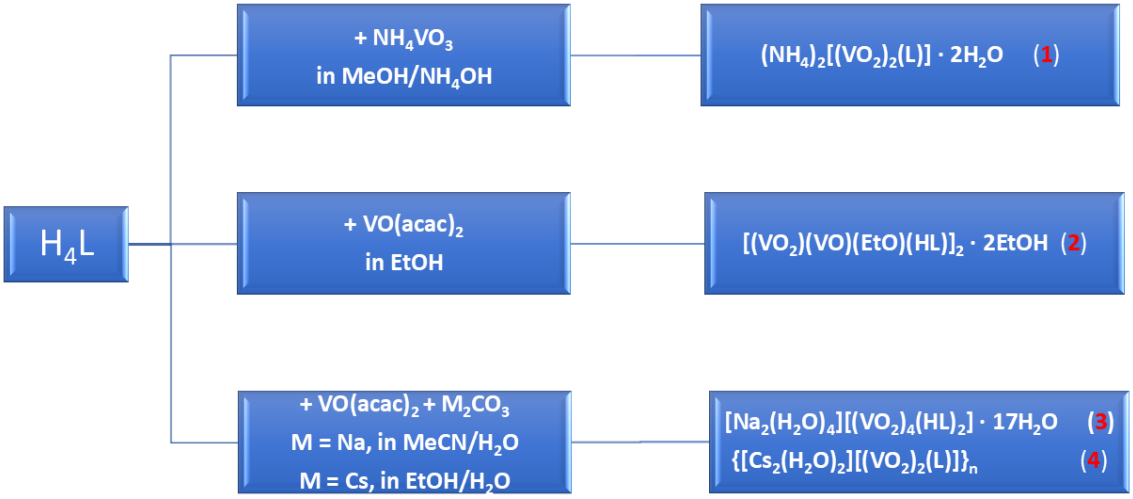

Scheme S1. Synthesis of compounds **1-4**.

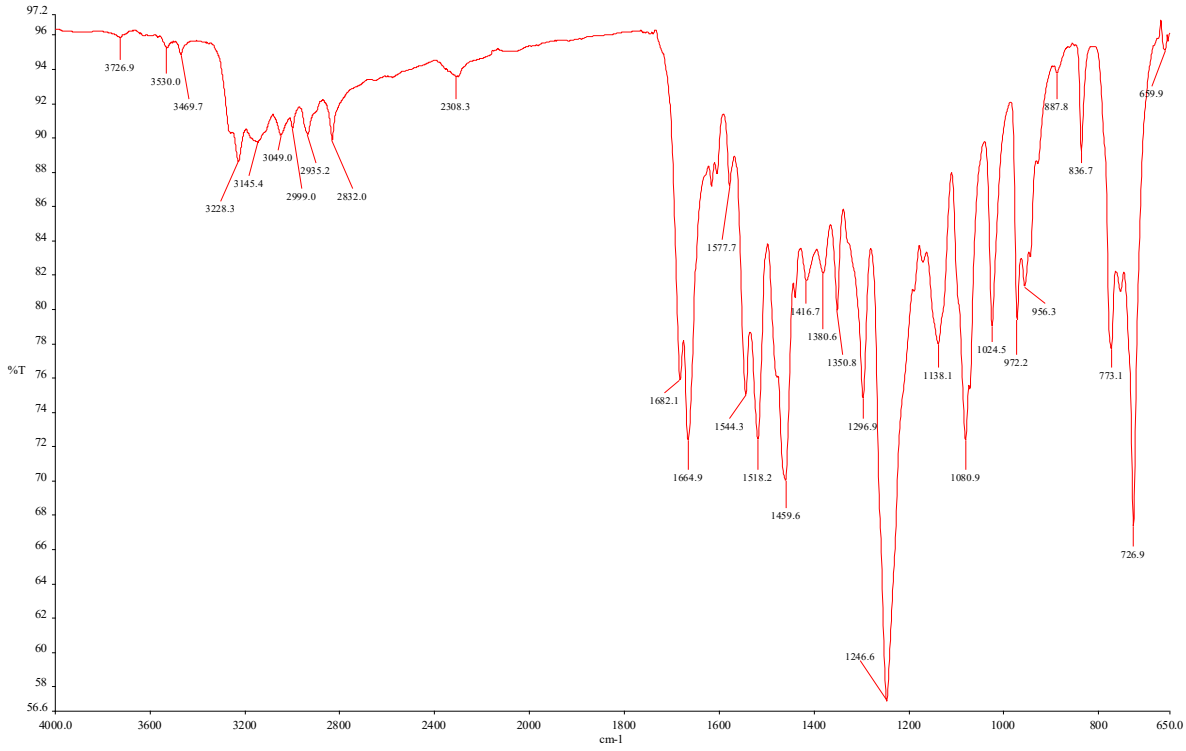

Fig. S1. IR spectrum of H_4L ligand.

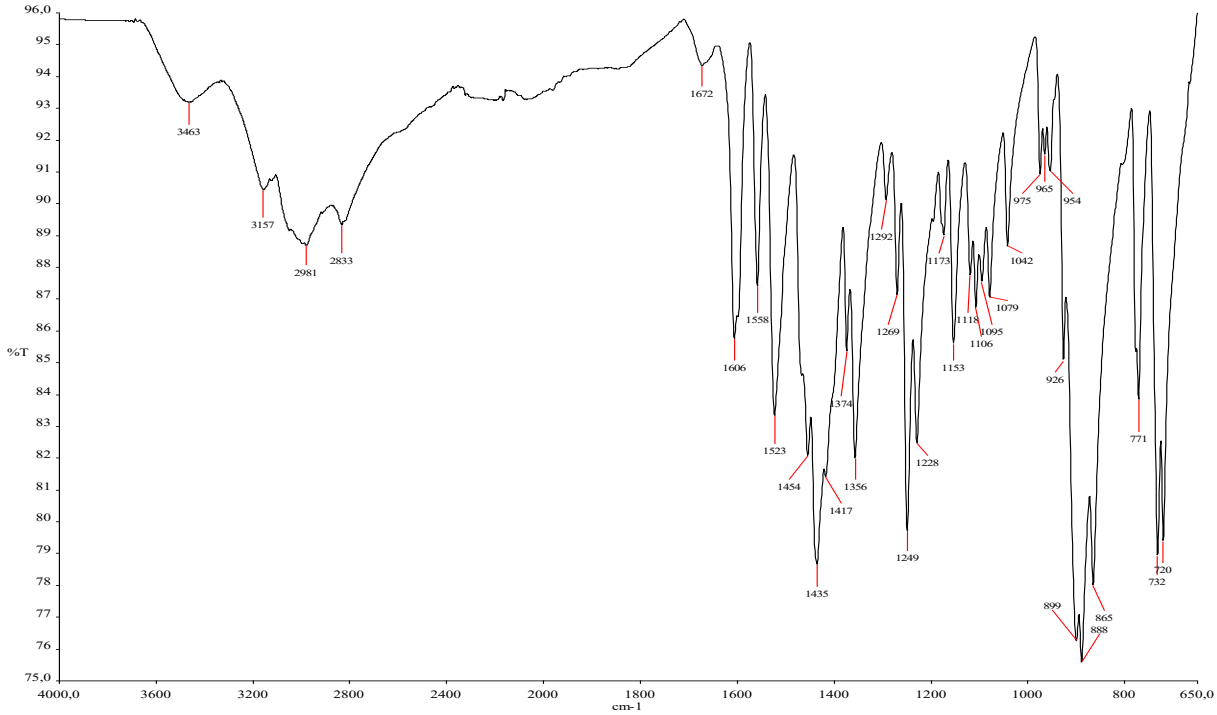

Fig. S2. IR spectrum of **1**.

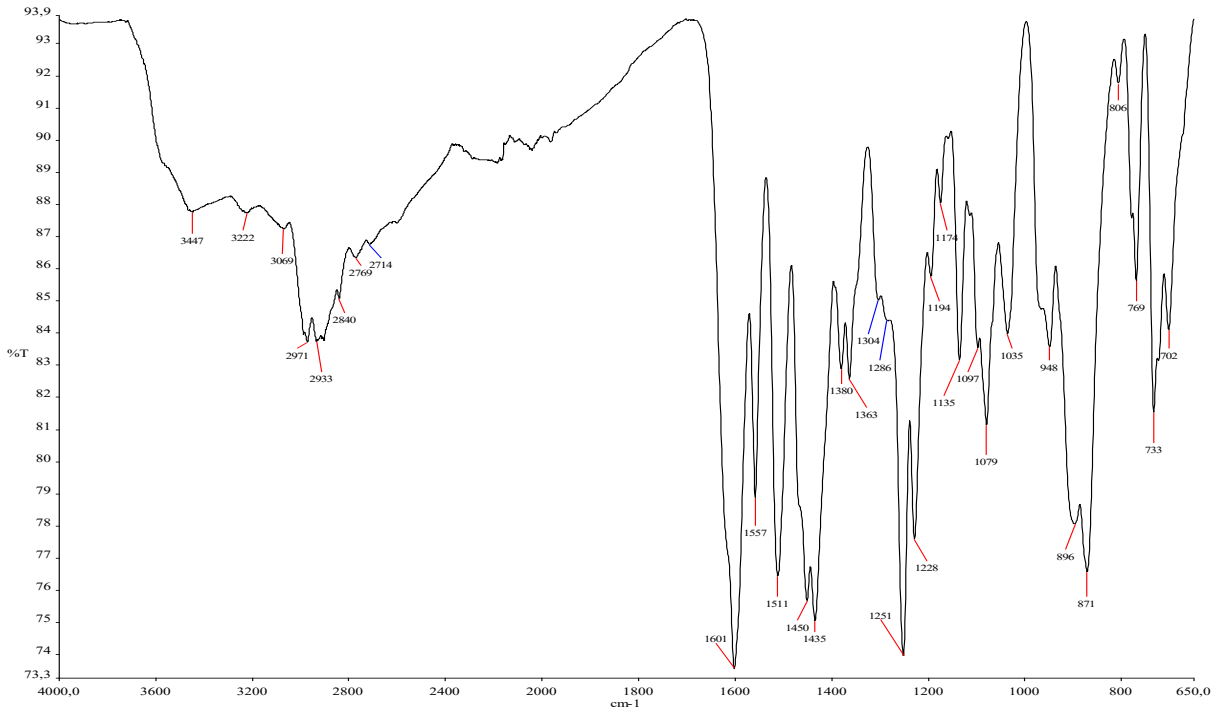

Fig. S3. IR spectrum of **2**.

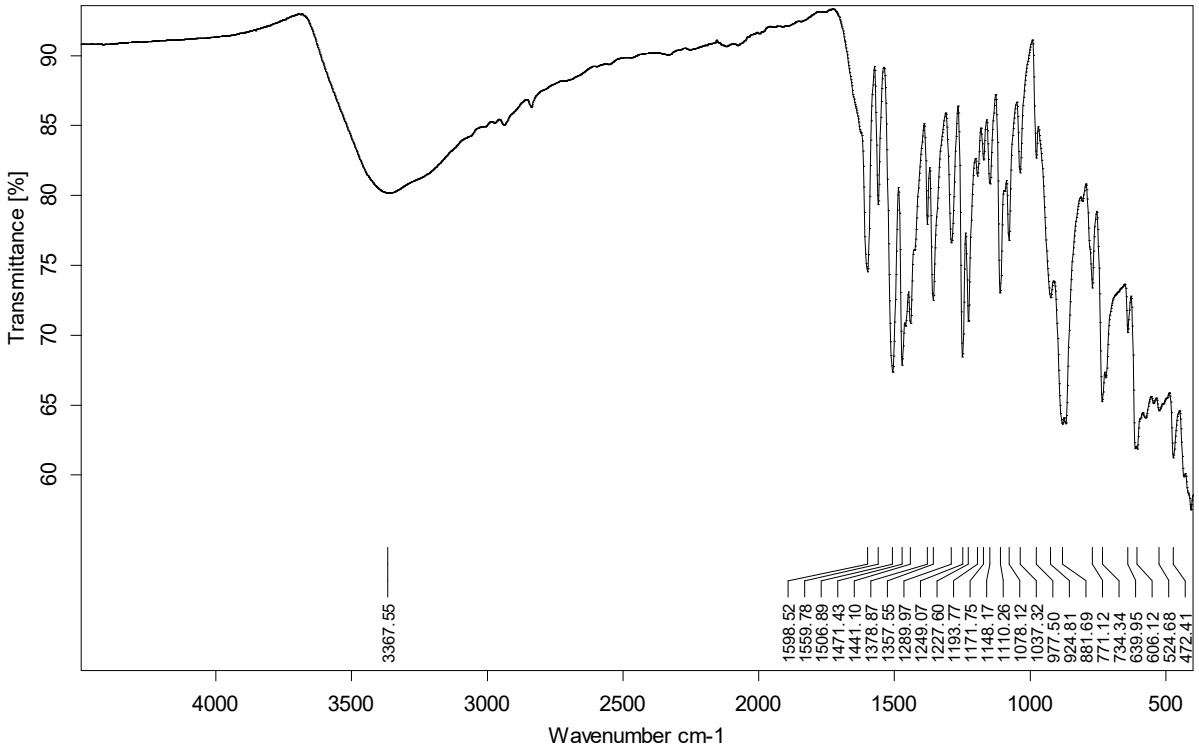

Fig. S4. IR spectrum of **3**.

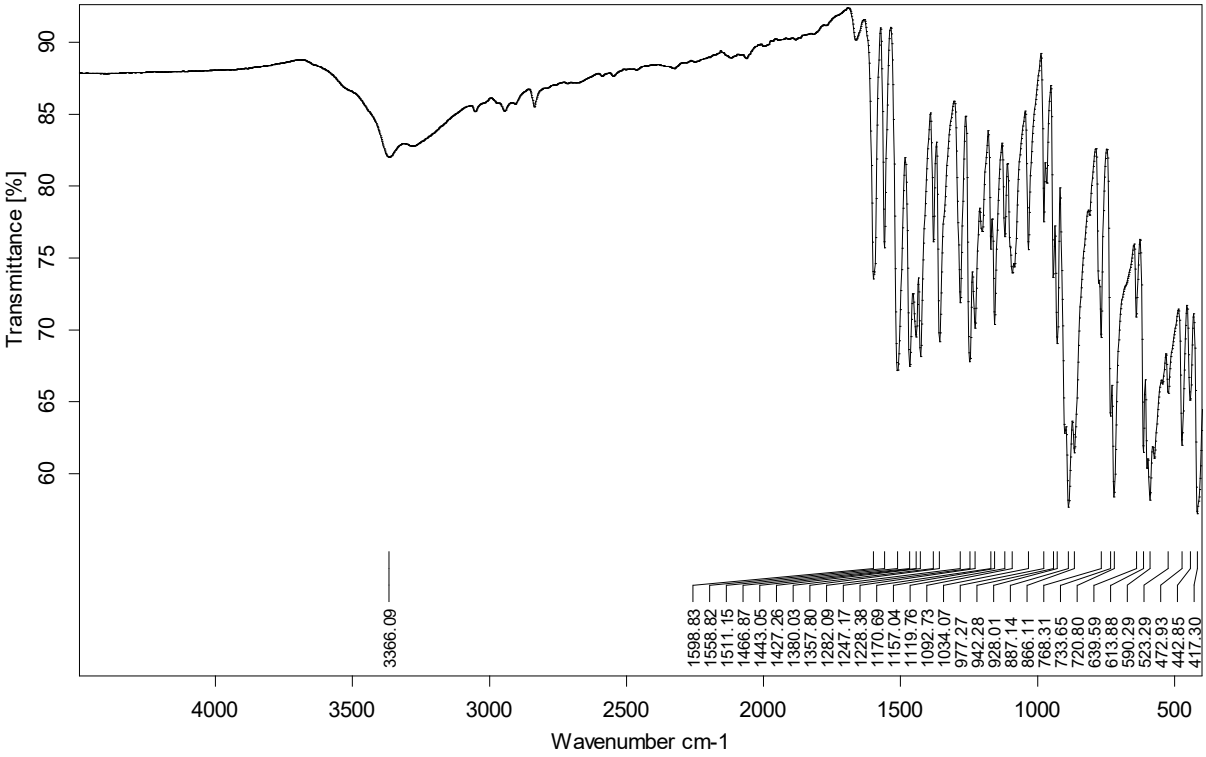

Fig. S5. IR spectrum of **4**.

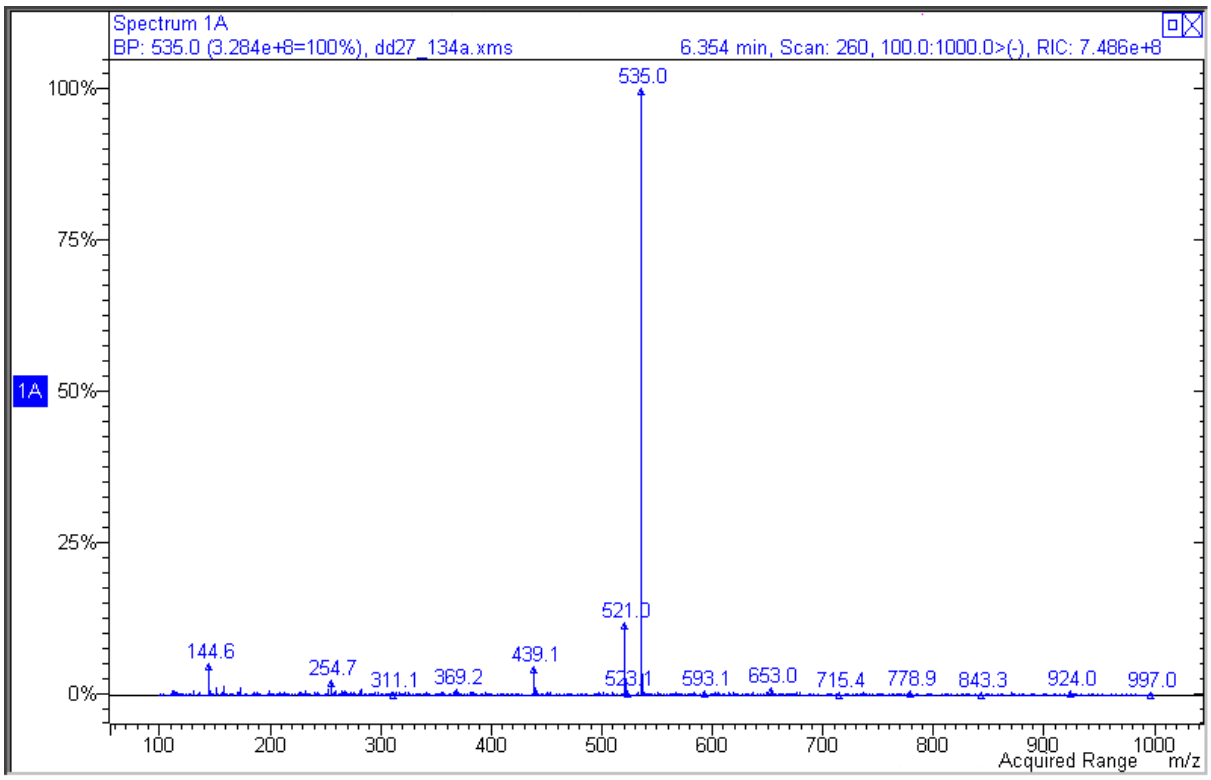

(a)

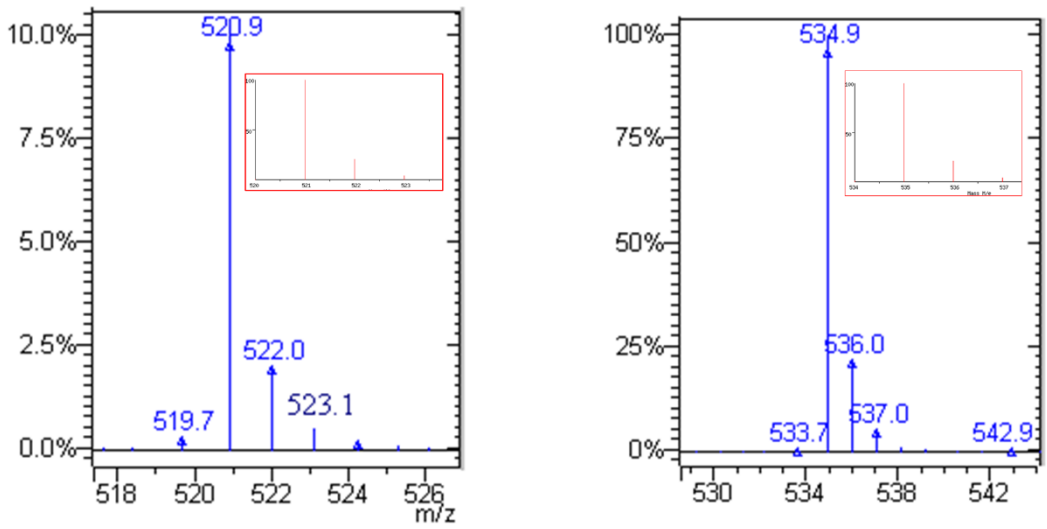

(b)

Fig. S6. (a) Negative-ion ESI mass spectrum of **1** in MeOH. (b) Experimental and simulated (insert) isotope patterns for the anionic fragments $[(VO_2)_2(HL)]^-$ (*m*/*z* 521) and $[(VO_2)(VO)(L)(CH_3O)]^-$ (*m*/*z* 535) in **1**.

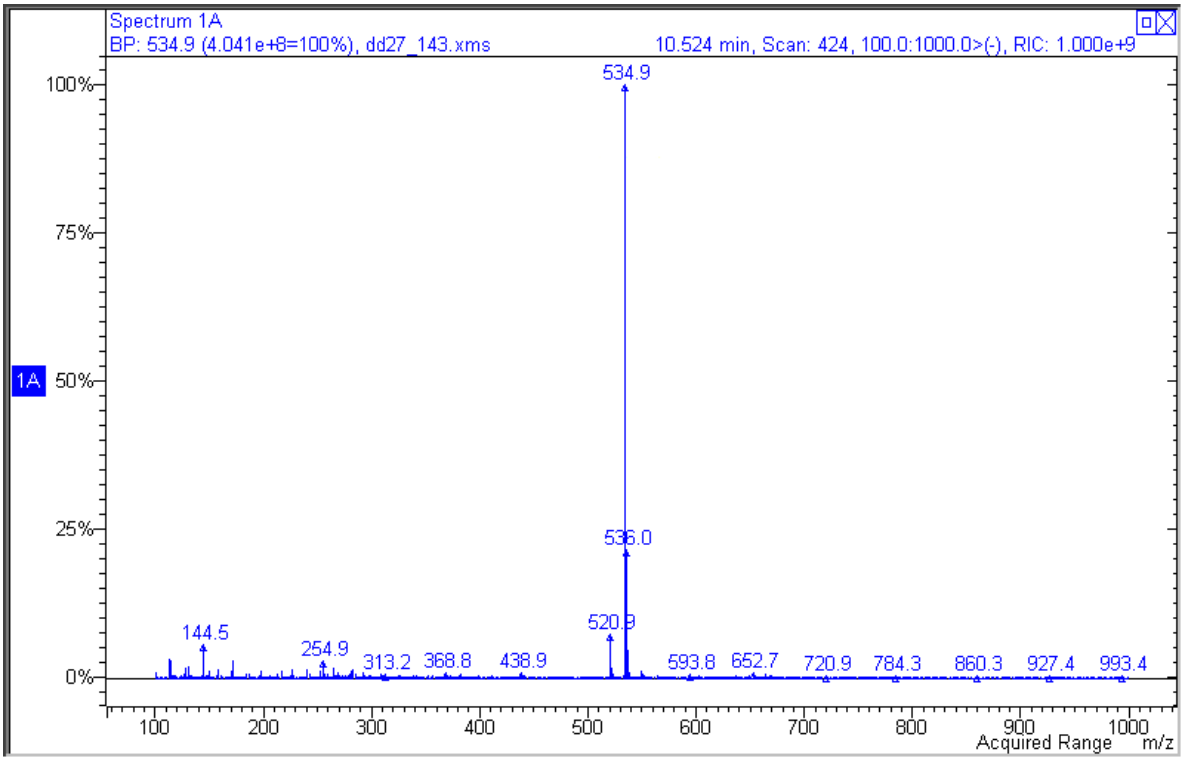

(a)

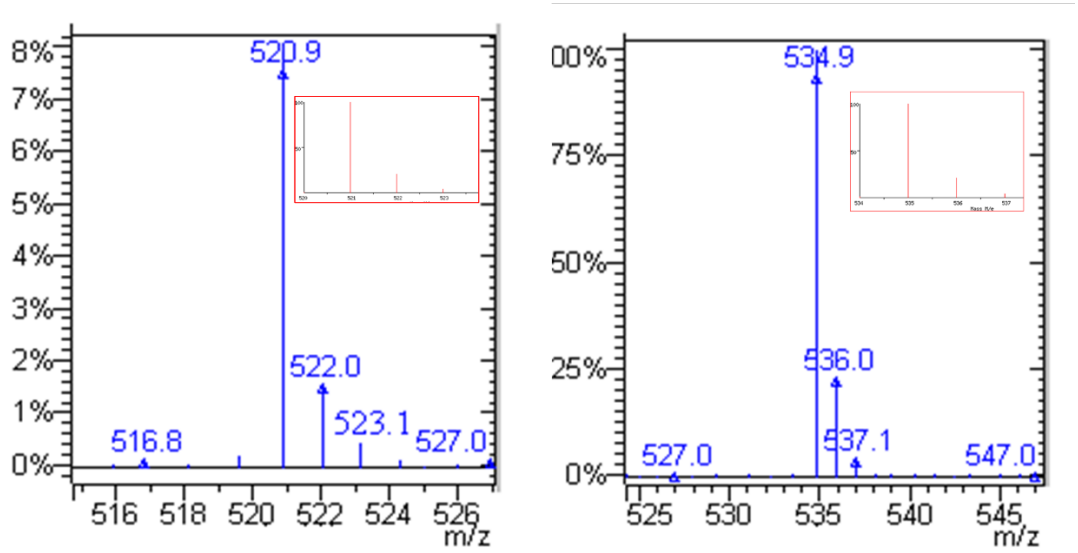

(b)

Fig. S7. (a) Negative-ion ESI mass spectrum of **2** in MeOH. (b) Experimental and simulated (insert) isotope patterns for the anionic fragments $[(VO_2)_2(HL)]^-$ (*m*/*z* 521) and $[(VO_2)(VO)(L)(CH_3O)]^-$ (*m*/*z* 535) in **2**.

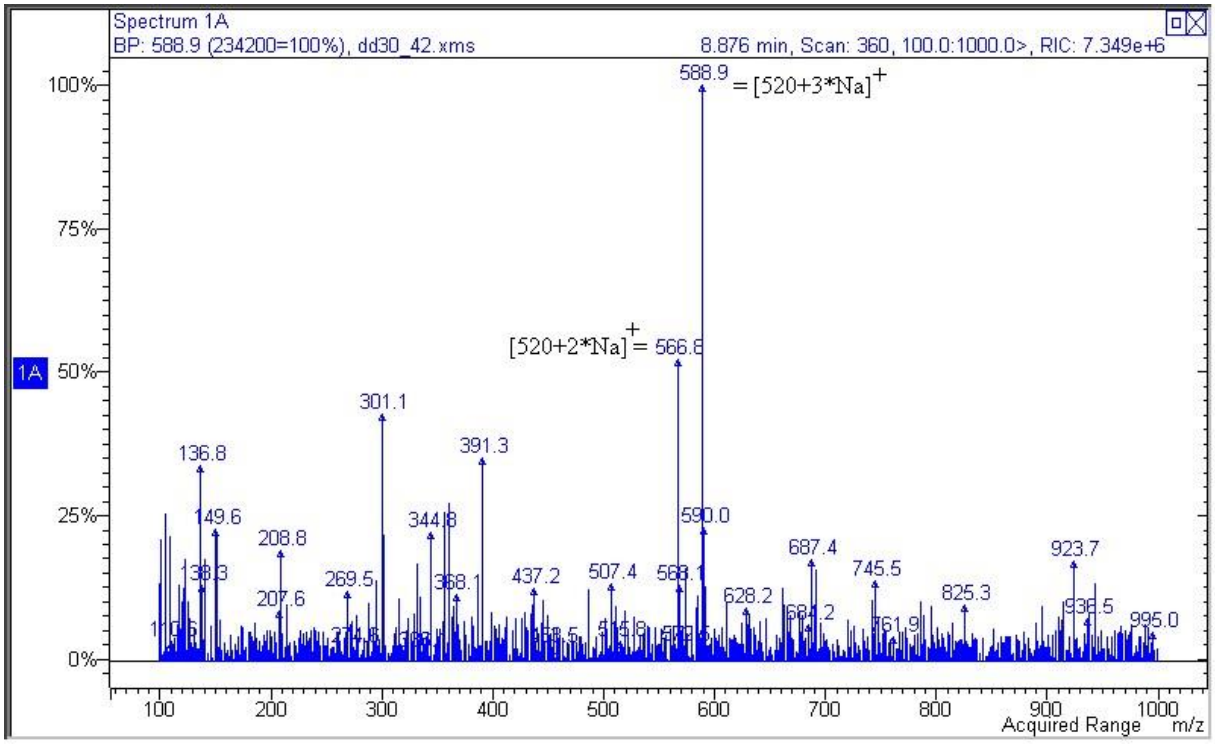

(a)

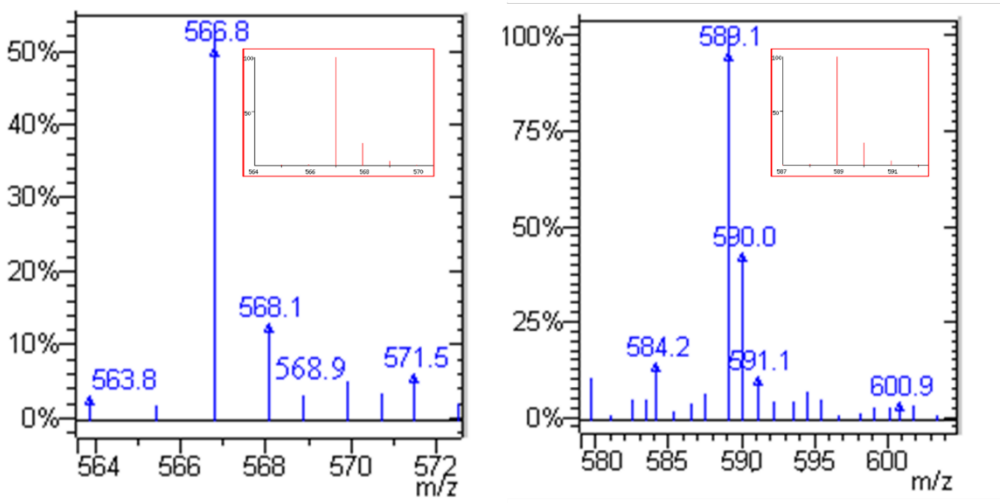

(b)

Fig. S8. (a) Positive-ion ESI mass spectrum of **3** in dmso. (b) Experimental and simulated (insert) isotope patterns for the cationic fragments $\{[(VO_2)_2(L)]+2Na\}^+$ (*m*/*z* 567) and $\{[(VO_2)_2(L)]+3Na\}^+$ (*m*/*z* 589) in **3**.

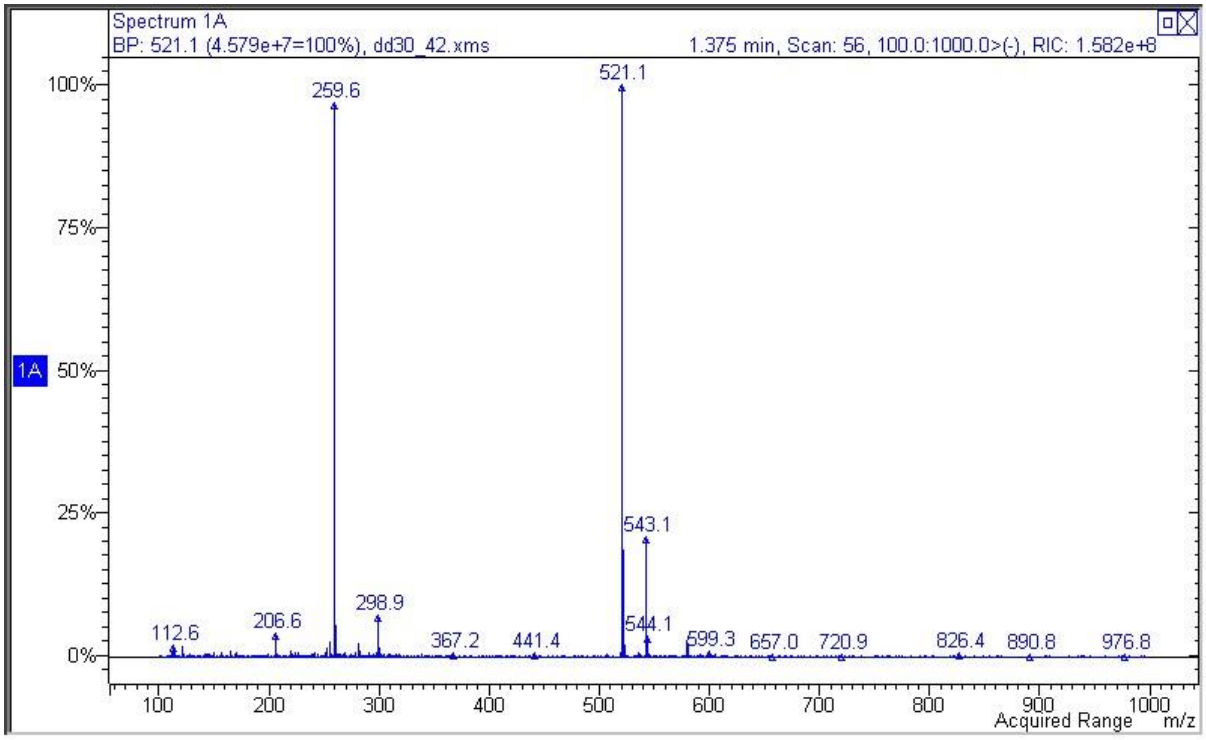

(a)

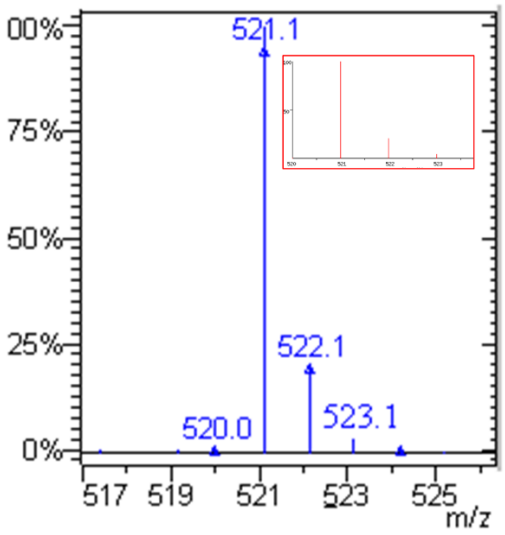

(b)

Fig. S9. (a) Negative-ion ESI mass spectrum of **3** in dmso. (b) Experimental and simulated (insert) isotope patterns for the anionic fragment $[(VO_2)_2(HL)]^-$ (*m*/*z* 521) in **3**.

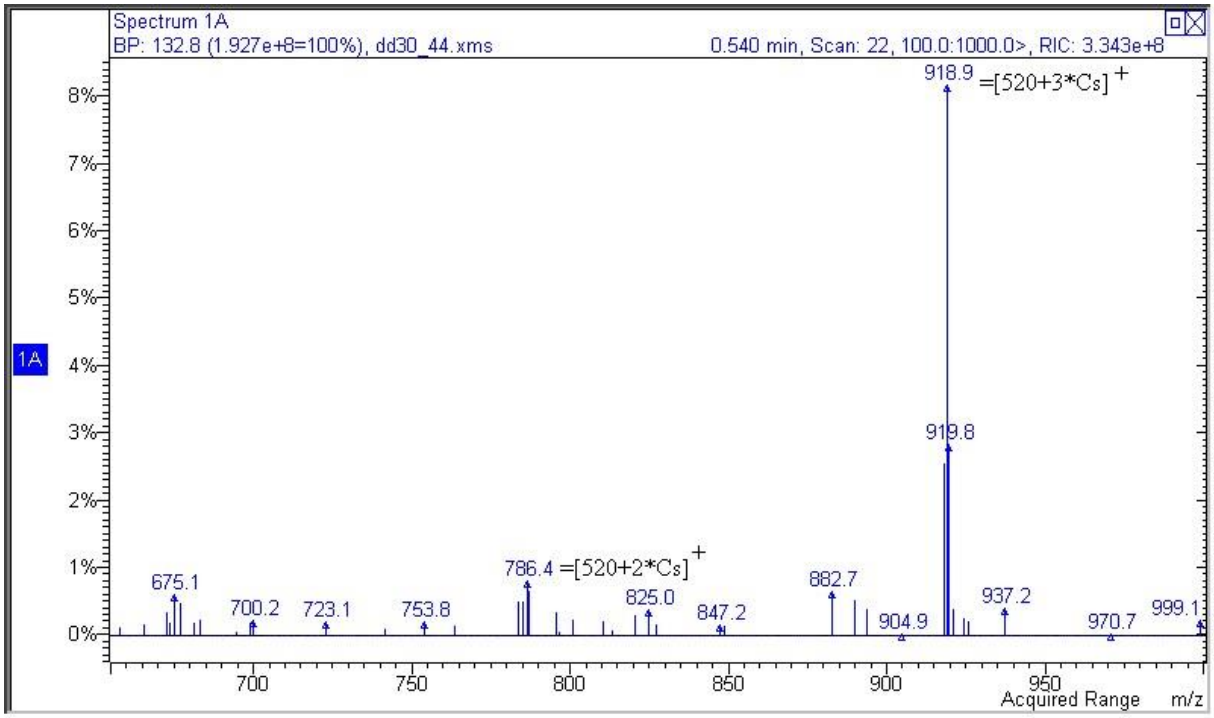

(a)

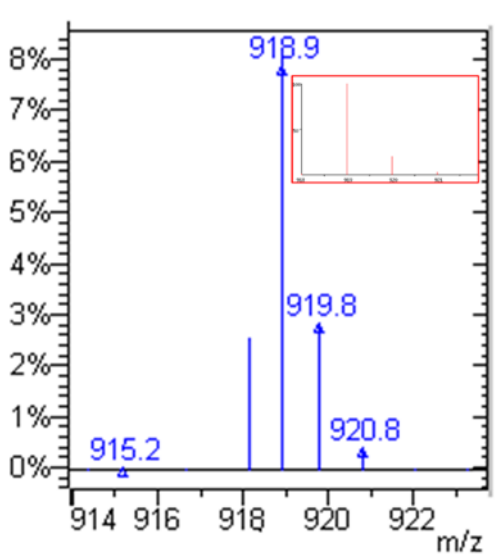

(b)

Fig. S10. (a) Positive-ion ESI mass spectrum of **4** in dmso. (b) Experimental and simulated (insert) isotope patterns for the cationic fragment $\{[(VO_2)_2(L)]+3Cs\}^+$ (*m/z* 919) in **4**.

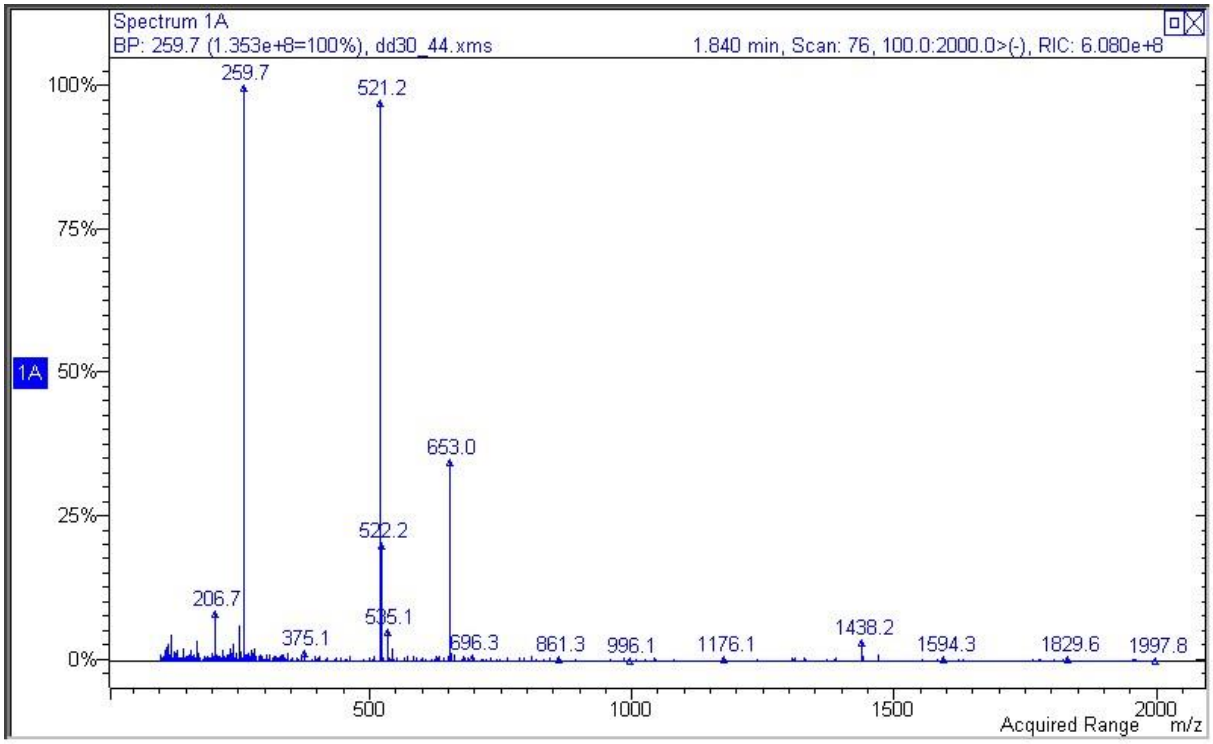

(a)

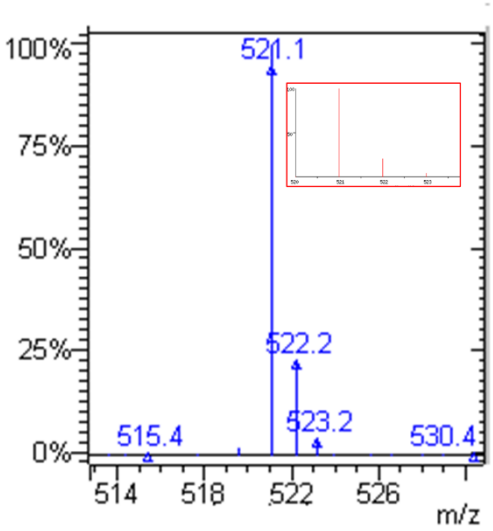

(b)

Fig. S11. (a) Negative-ion ESI mass spectrum of **4** in dmso. (b) Experimental and simulated (insert) isotope patterns for the anionic fragment $[(VO_2)_2(HL)]^-$ (*m*/*z* 521) in **4**.

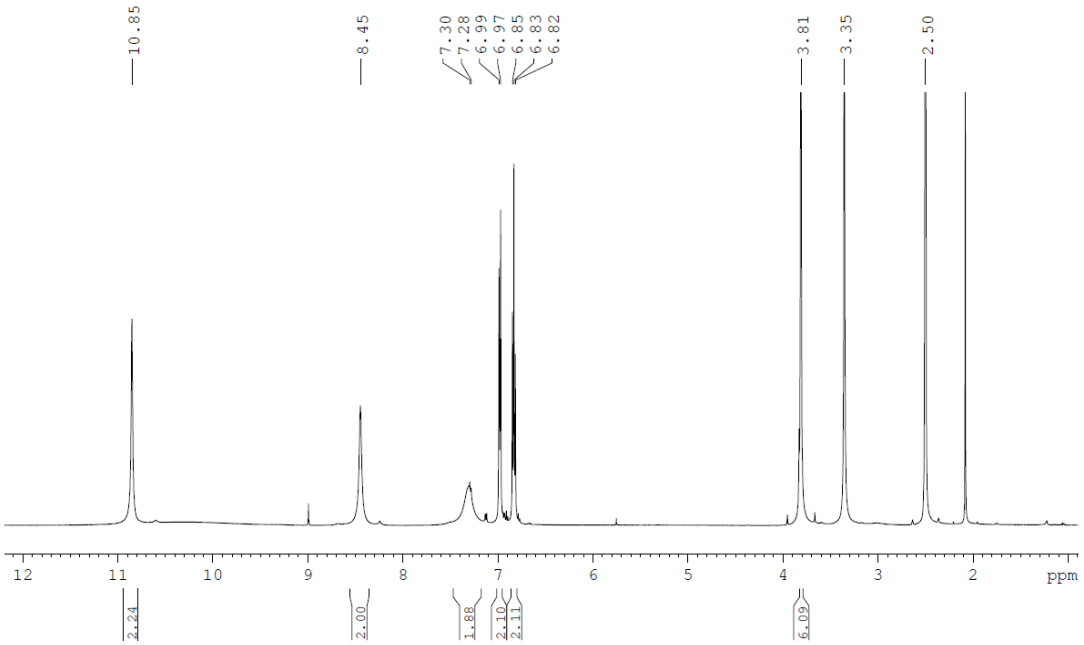

Fig. S12. ^{1}H NMR spectrum of 1,5-bis(2-hydroxy-3-methoxybenzylidene)carbohydrazide (H_4L).

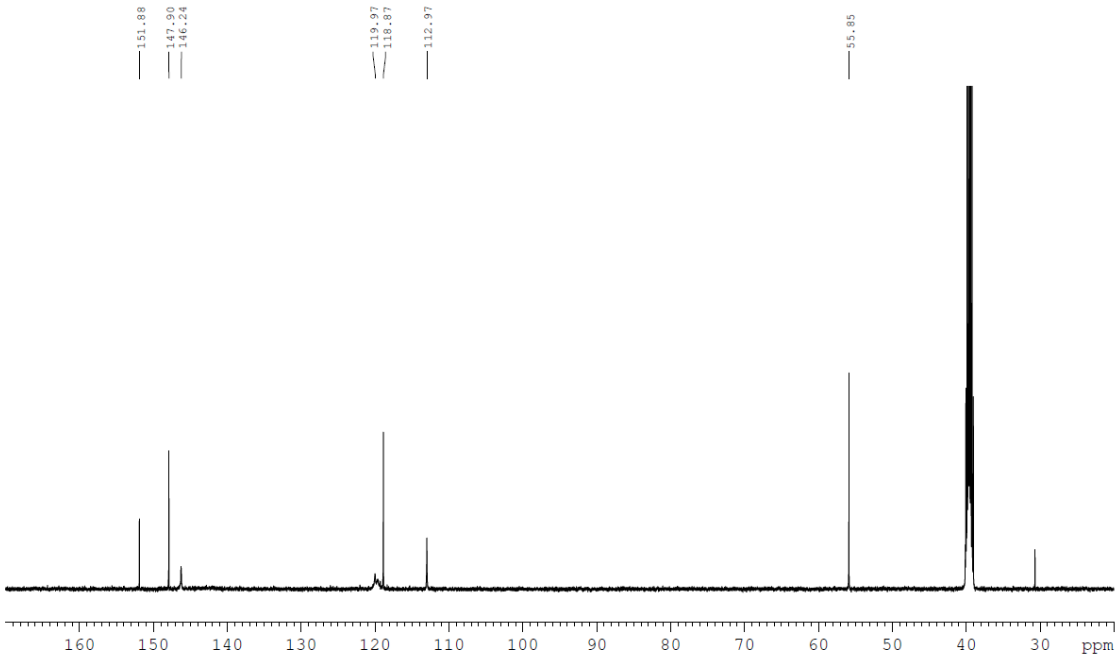

Fig. S13. ^{13}C NMR spectrum of 1,5-bis(2-hydroxy-3-methoxybenzylidene)carbohydrazide (H_4L).

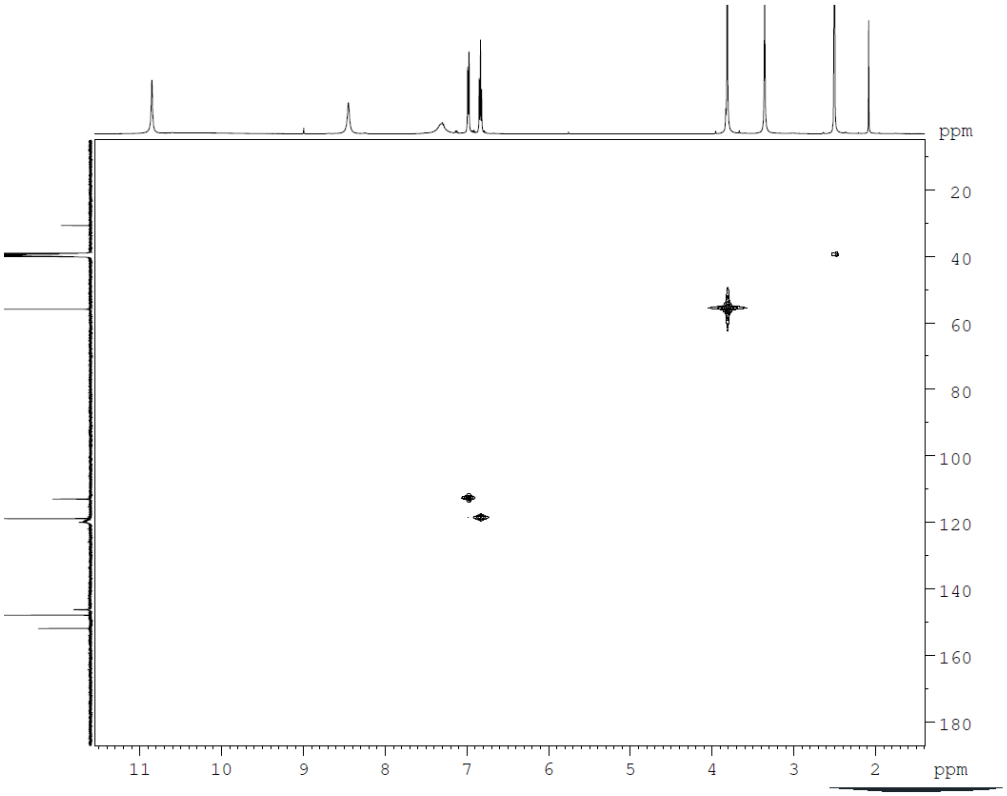

Fig. S14. $^{1}H/\ ^{13}C$ qHSQC NMR spectrum of H_4L.

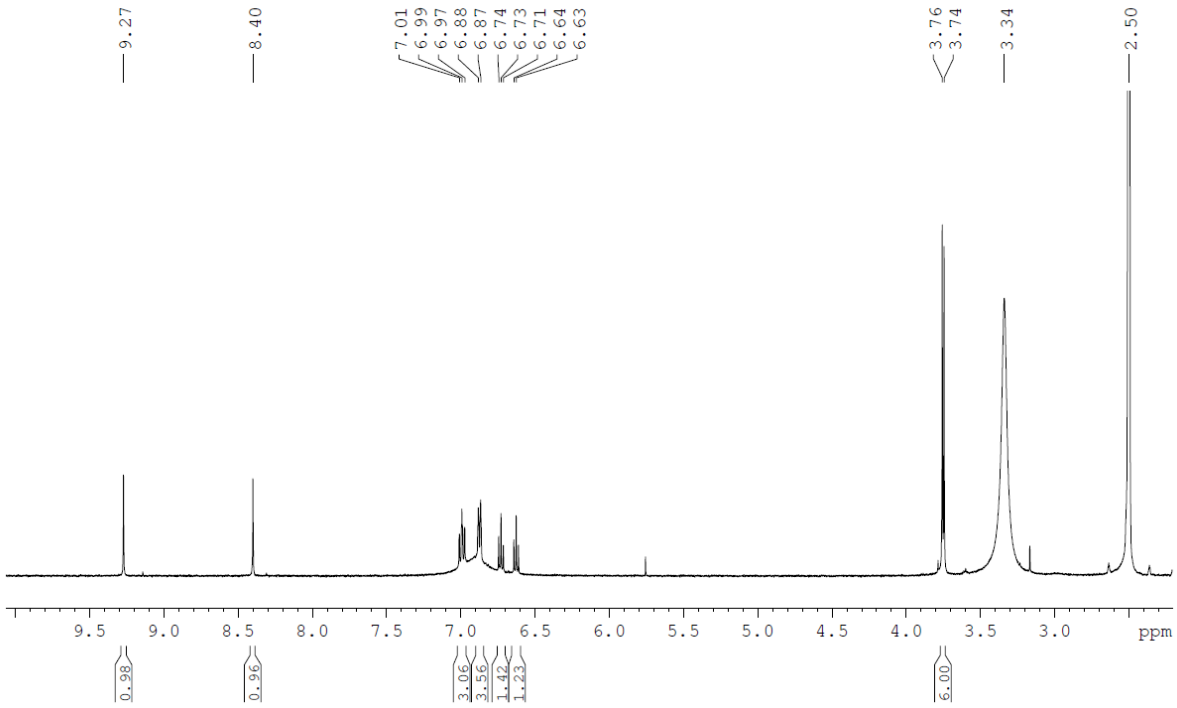

Fig. S15. ^{1}H NMR spectrum of **1**.

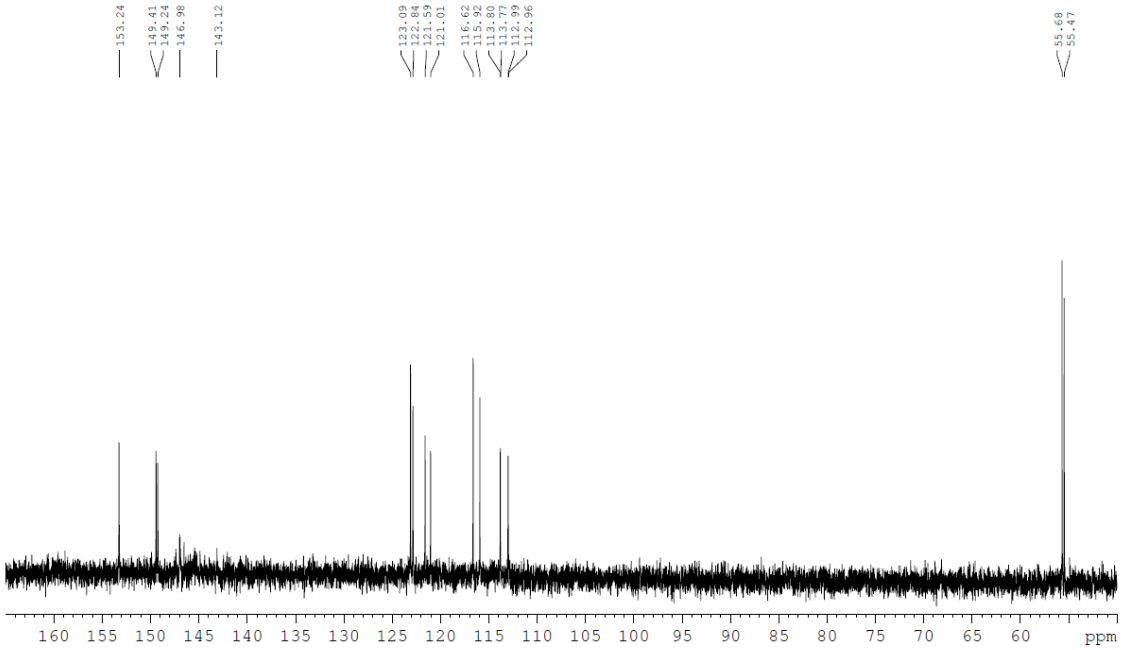

Fig. S16. ^{13}C NMR spectrum of **1**.

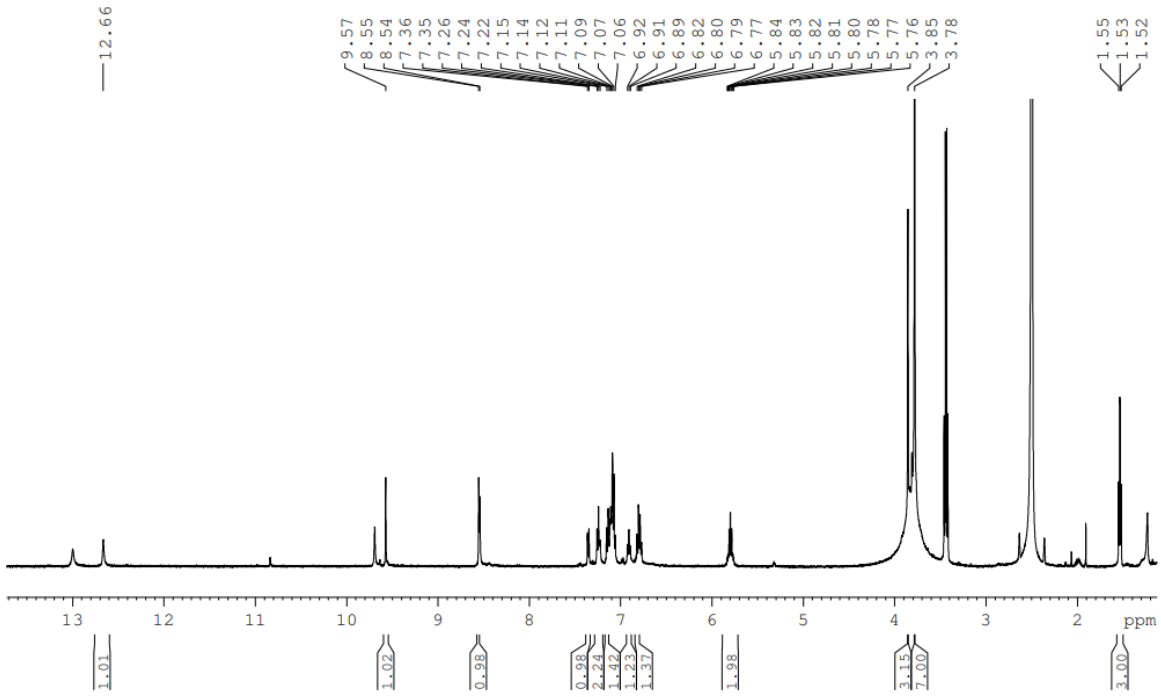

Fig. S17. ^{1}H NMR spectrum of **2**.

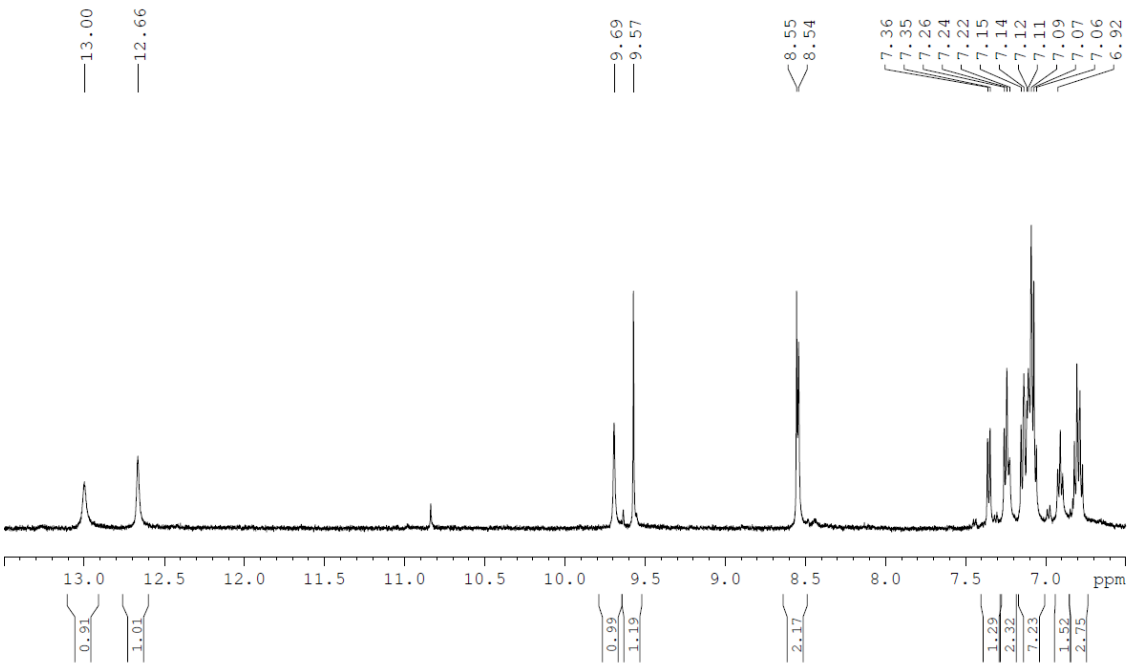

Fig. S18. ^{1}H NMR spectrum of **2** (showing hydrazinic protons and aromatic region).

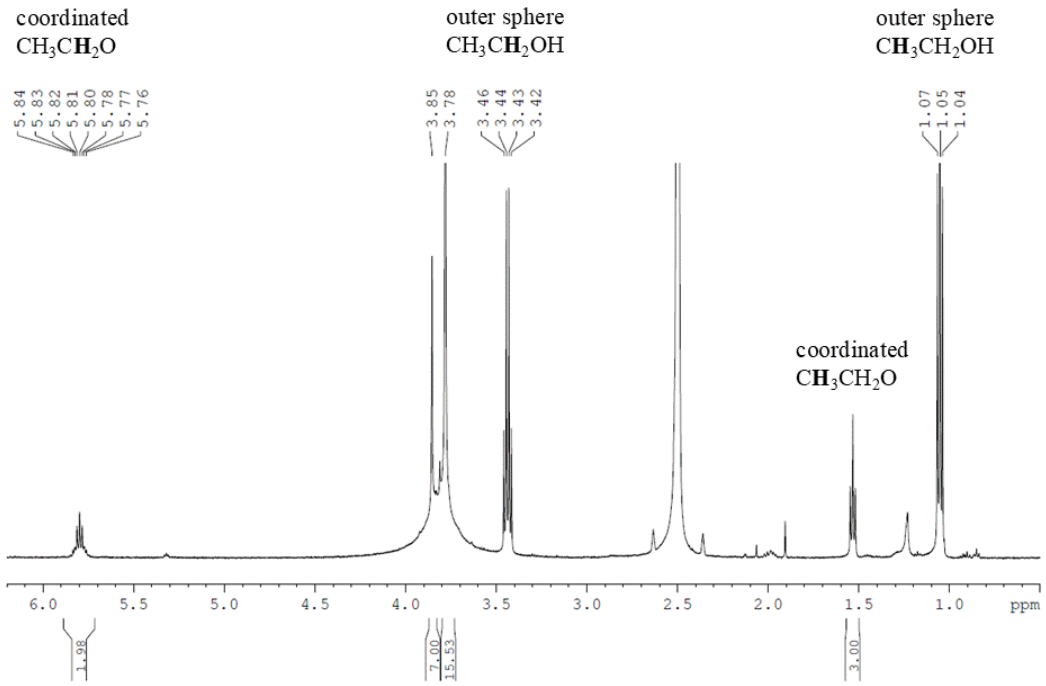

Fig. S19. ^{1}H NMR spectrum of **2** (aliphatic region).

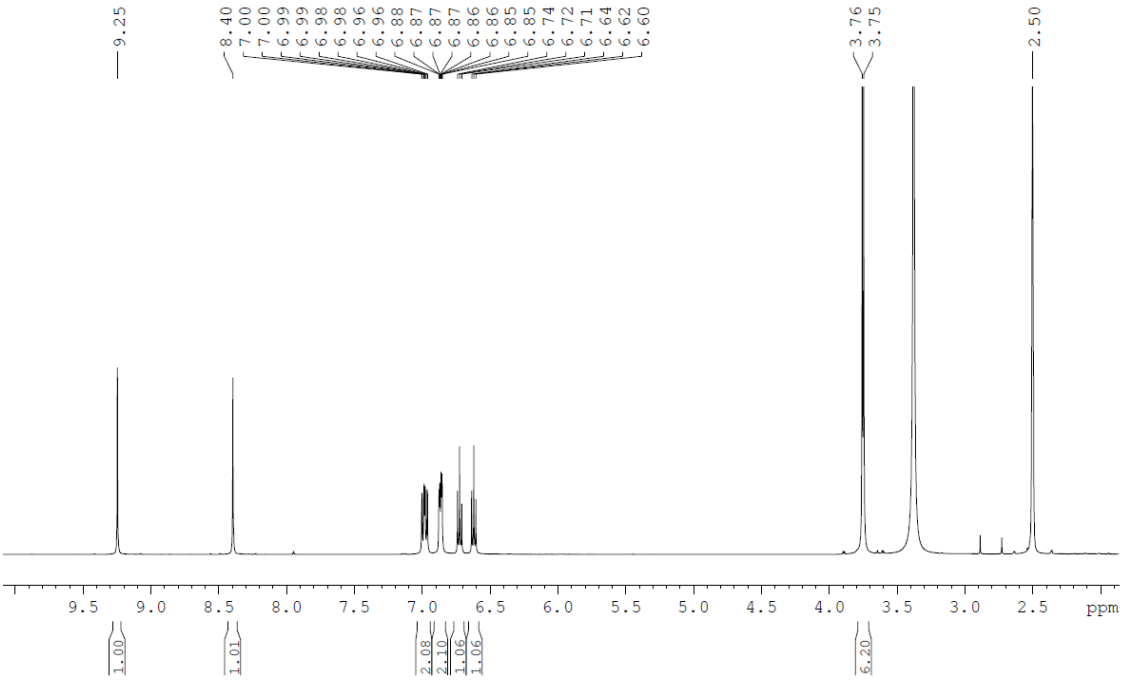

Fig. S20. ^{1}H NMR spectrum of **3**.

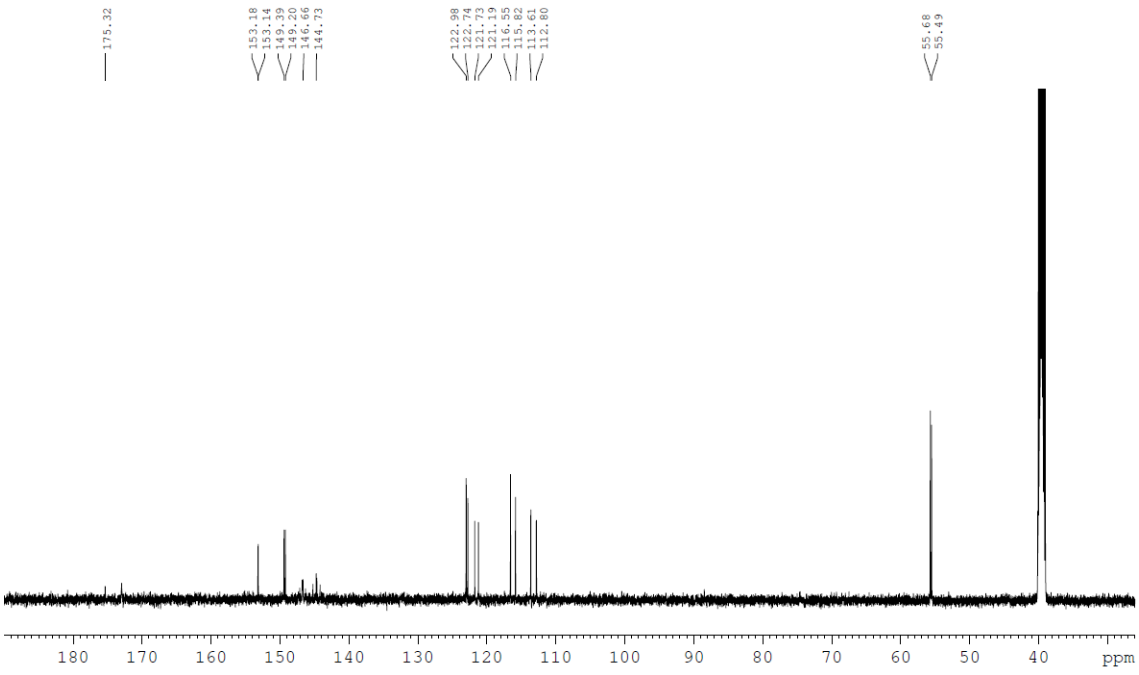

Fig. S21. ^{13}C NMR spectrum of **3**.

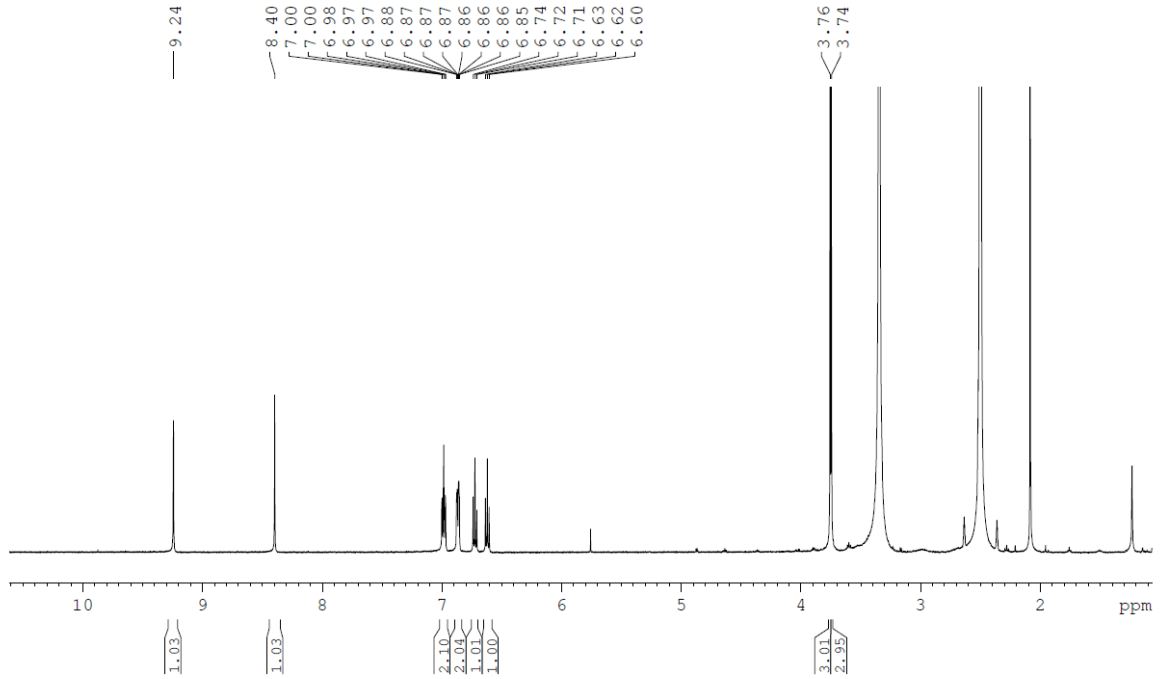

Fig. S22. ^{1}H NMR spectrum of **4**.

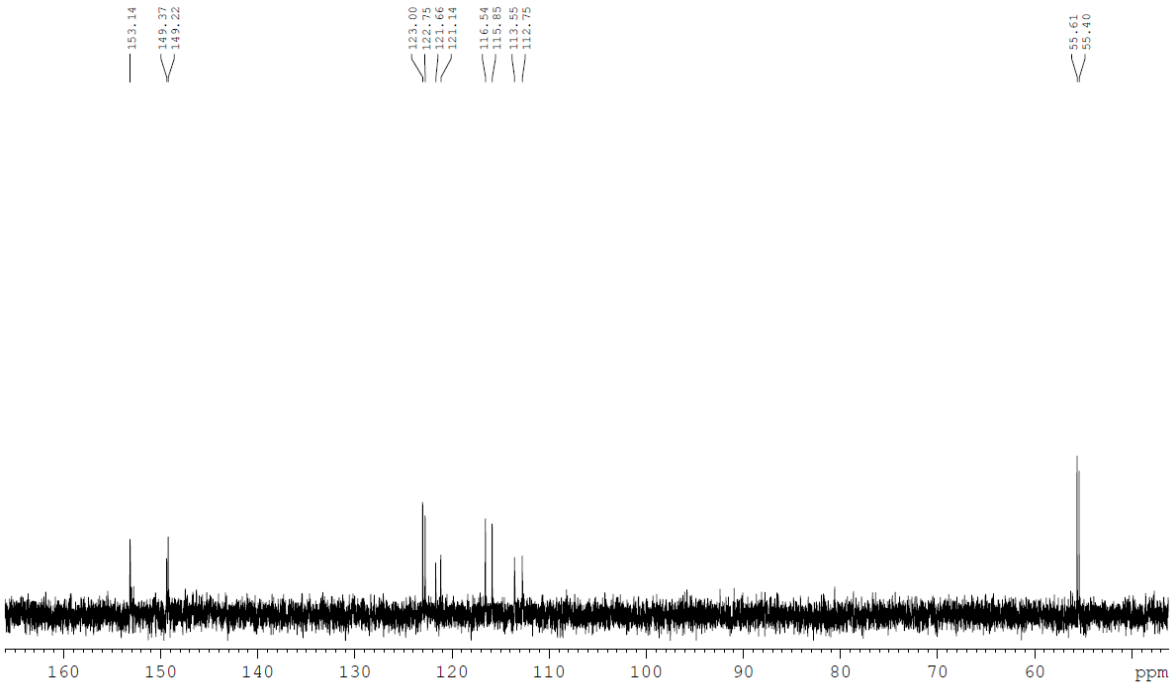

Fig. S23. ^{13}C NMR spectrum of **4**.

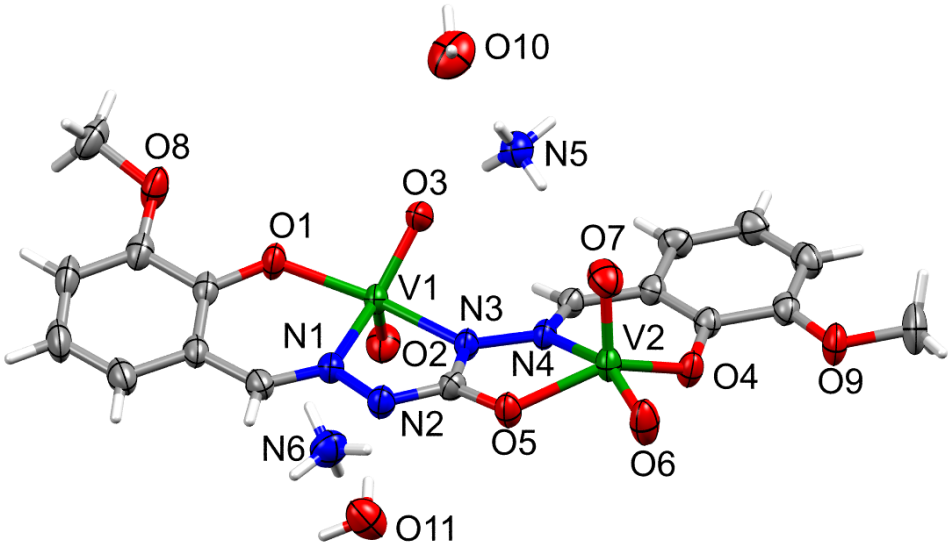

Fig. S24. The asymmetric unit of **1** with thermal ellipsoids shown at the 50% probability level and partial atom numbering.

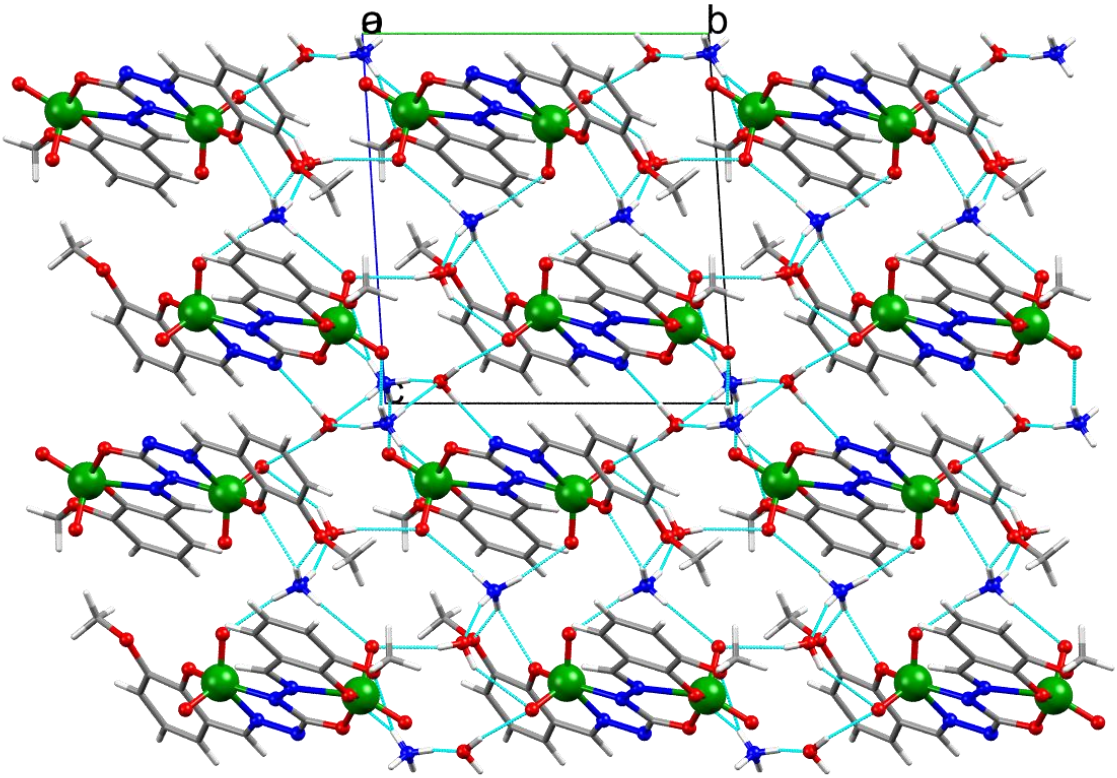

Fig. S25. 3D supramolecular network formed via N–H···O and O–H···O intermolecular hydrogen bonds in **1**.

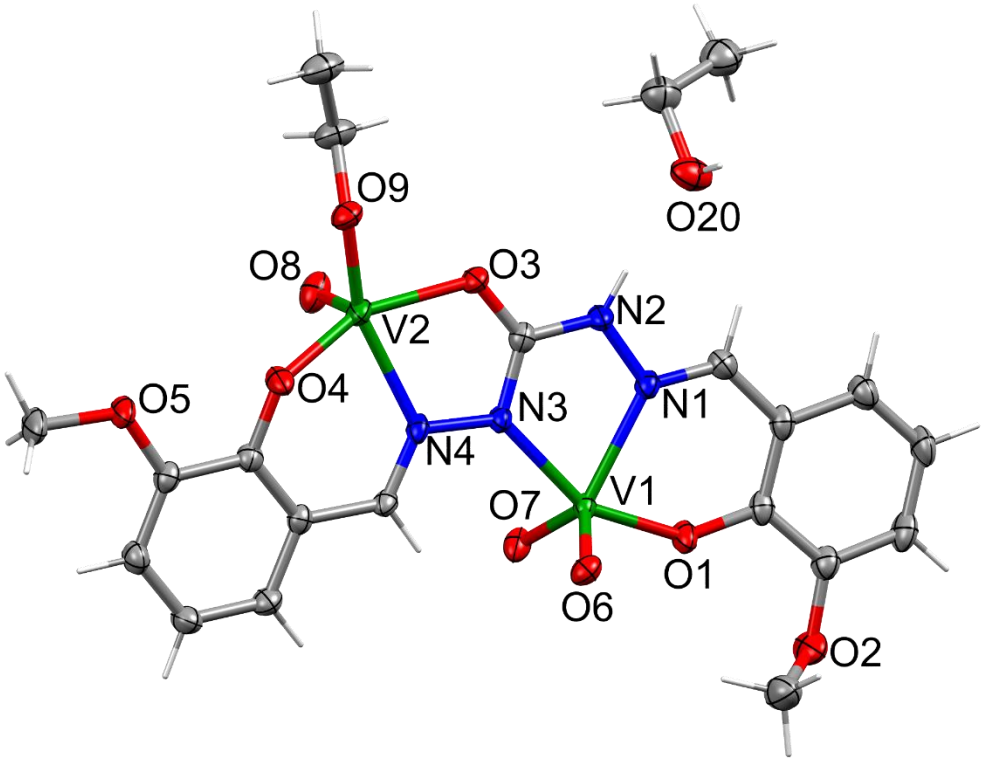

Fig. S26. The asymmetric unit of **2** with thermal ellipsoids shown at the 50% probability level and partial atom numbering.

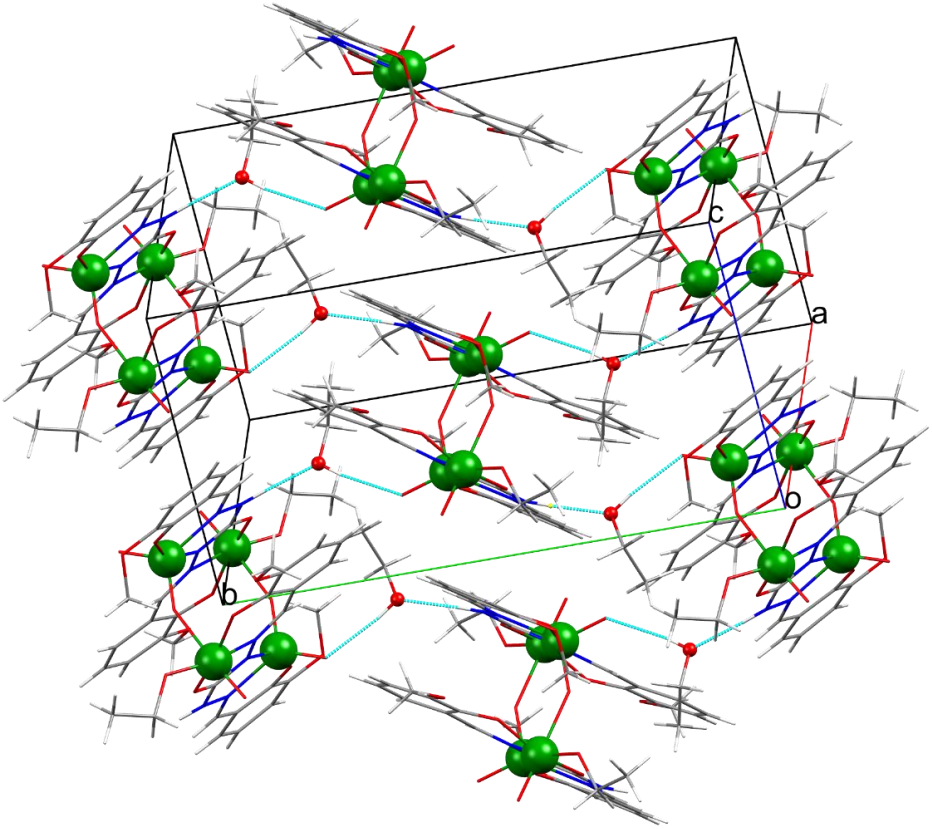

(a)

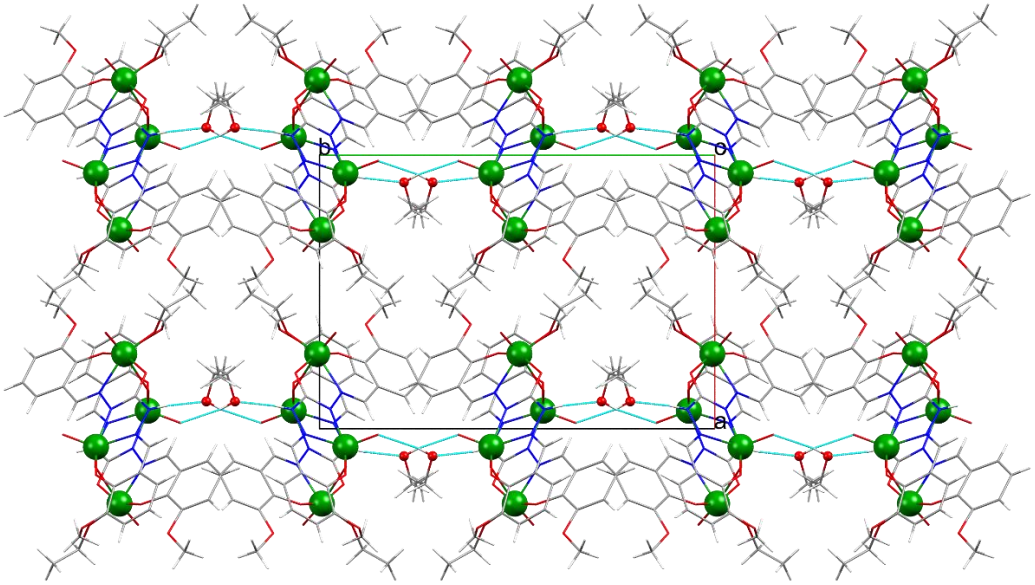

(b)

Fig. S27. The supramolecular layer formed via O–H…O and N–H…O hydrogen bonds between solvent EtOH molecules and tetranuclear V(V) clusters in **2** (a). The fragment of crystal structure of **2** viewed along the *b* axis (b). Hydrogen bonds are shown as blue dotted lines.

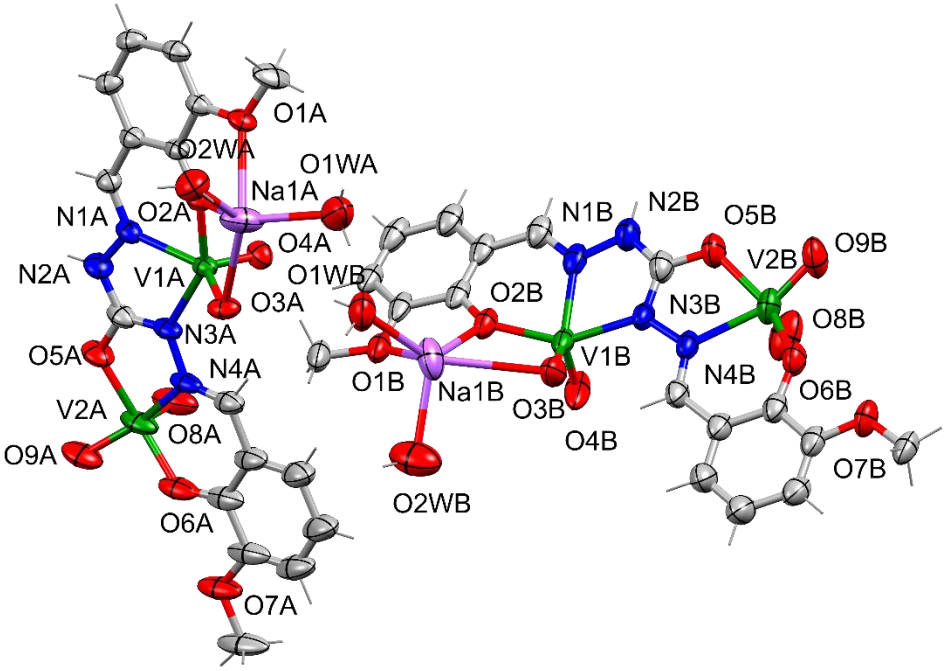

(a)

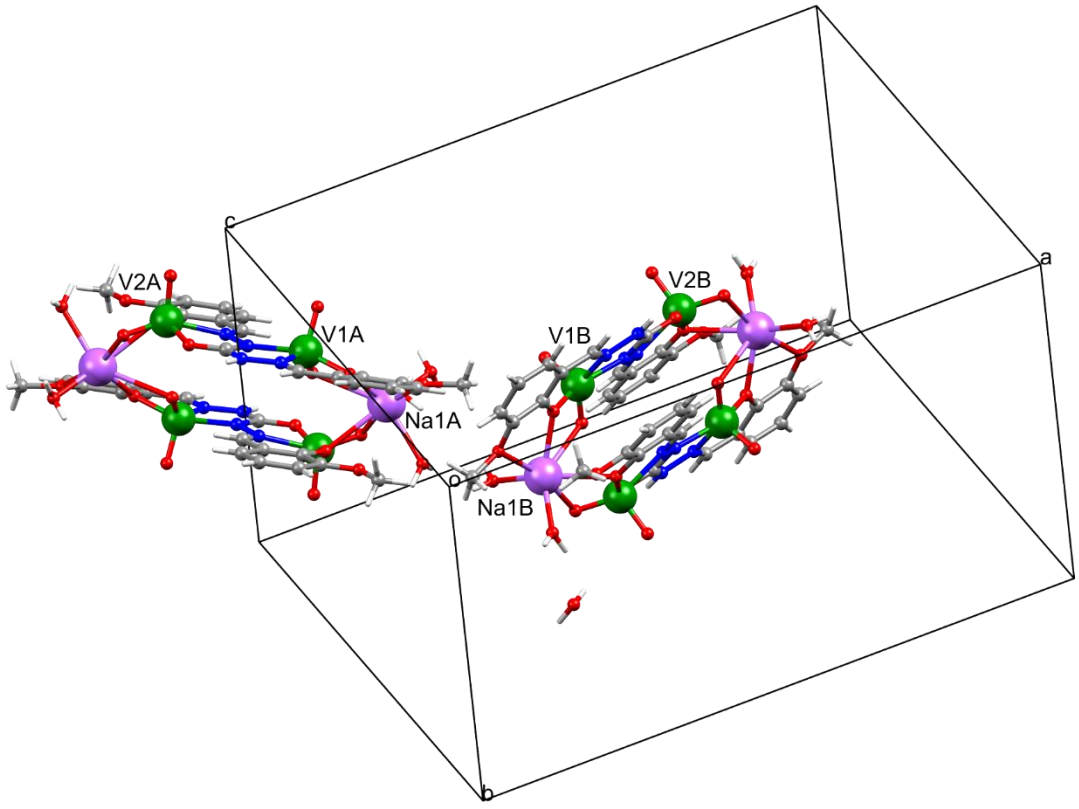

(b)

Fig. S28. The asymmetric unit of **3** with thermal ellipsoids shown at the 50% probability level (a). View of two crystallographic independent centrosymmetric neutral hexanuclear $[Na_2(H_2O)_4(VO_2)_4(HL)_2]$ clusters, denoted as A and B, and solvent water molecules in the unit cell of **3** (b).

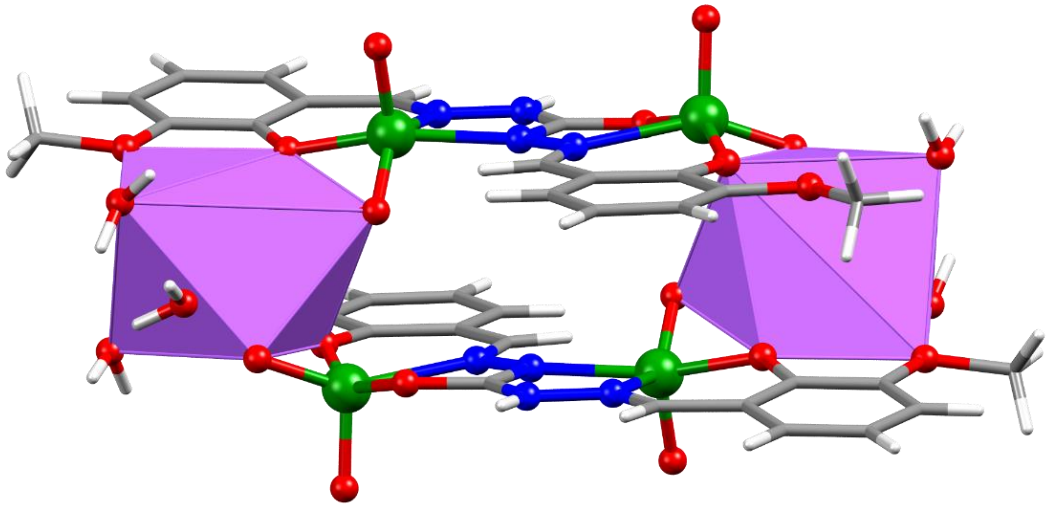

(a)

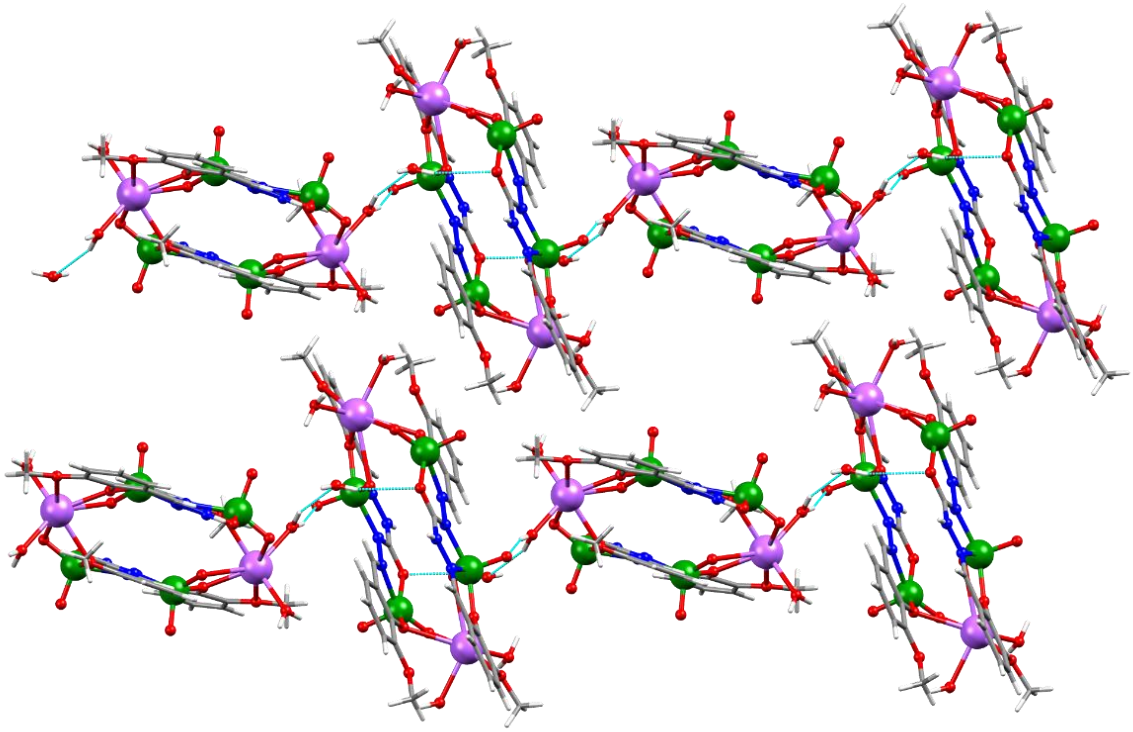

Fig. S29. View of a vanadium-based hexanuclear cluster with Na^+ cations highlighted in polyhedral mode formed in **3** (a). View of H-bonded chains formed in **3**. Hydrogen bonds are shown as blue dotted lines (b).

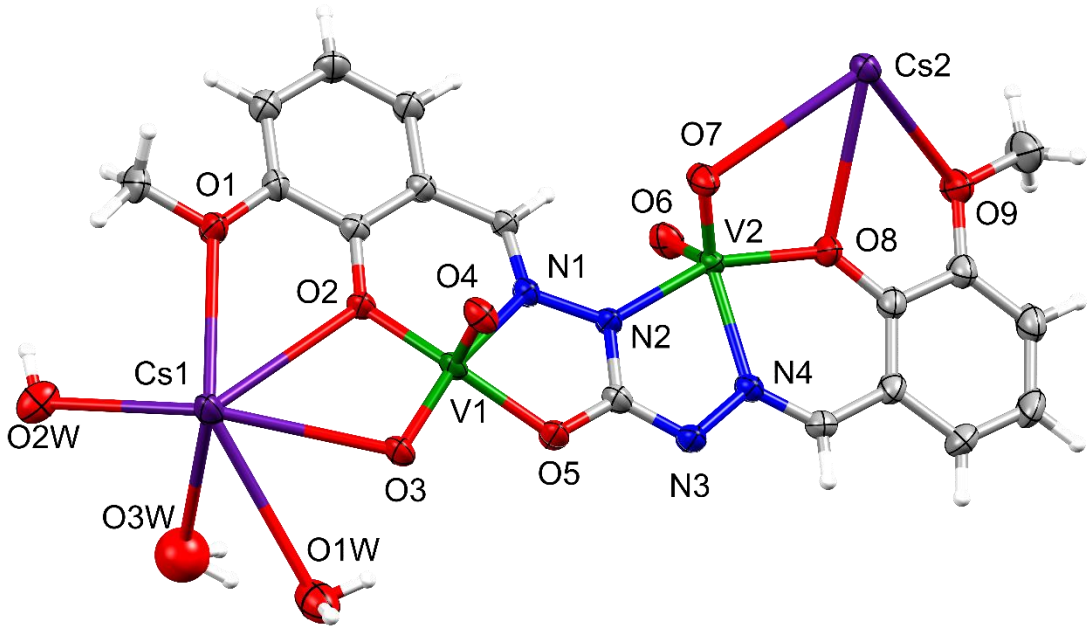

(a)

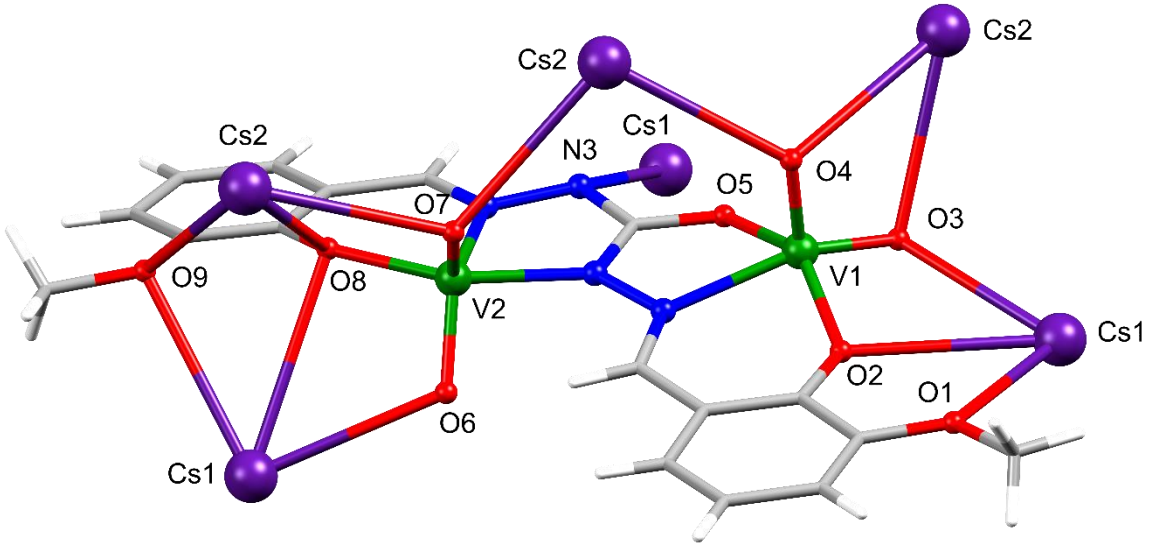

(b)

Fig. S30. The asymmetric unit of **4** with thermal ellipsoids shown at the 50% probability level and partial atom numbering (a). View of the $[(VO_2)_2(L)]^{2-}$ unit showing the coordination of all O and N donor sites of L^{4-} to the metal centers in the 3D polymeric structure of **4**.

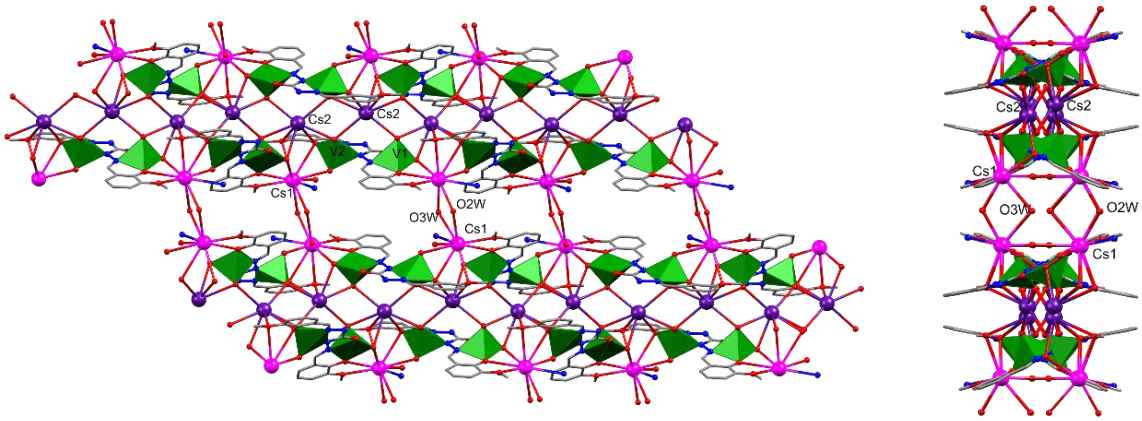

(a)

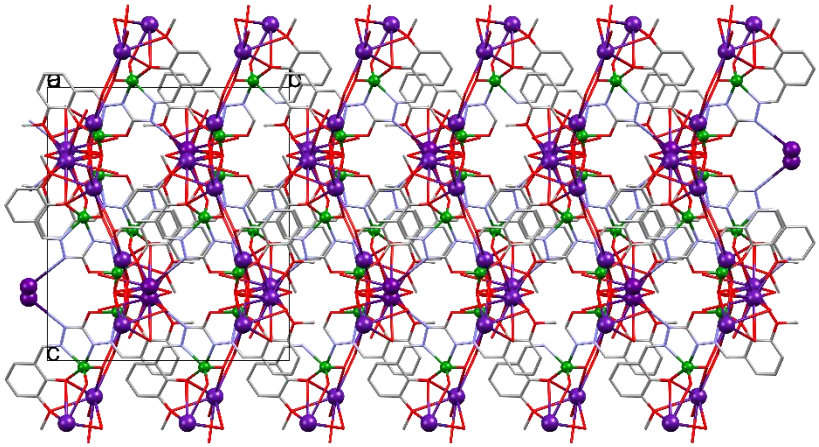

(b)

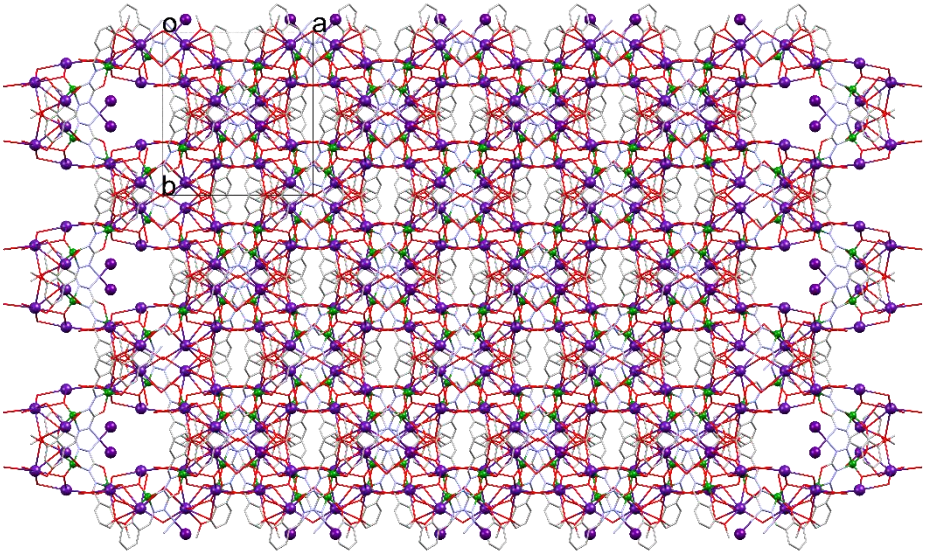

(c)

Fig. S31. Front and side views of the layers in **4**. Cs1 and Cs2 atoms are shown as pink and violet spheres, respectively, while V atoms are represented as green polyhedra (a). View of the 3D framework of **4** along the *a* axis (b) and the *c* axis (c).

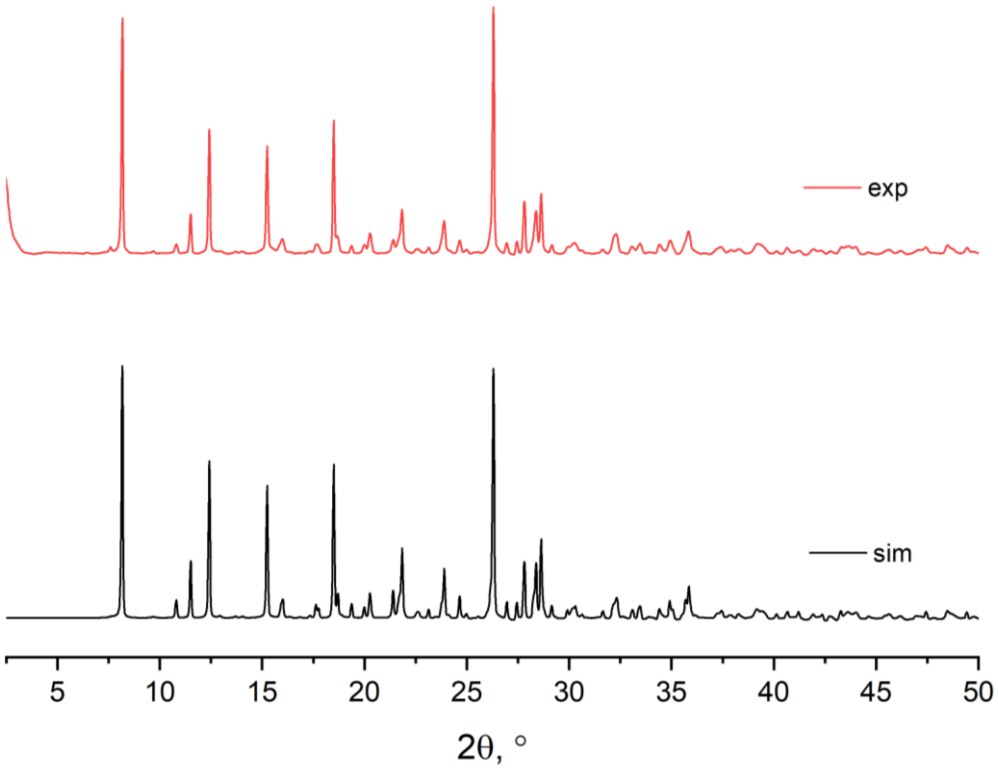

(a)

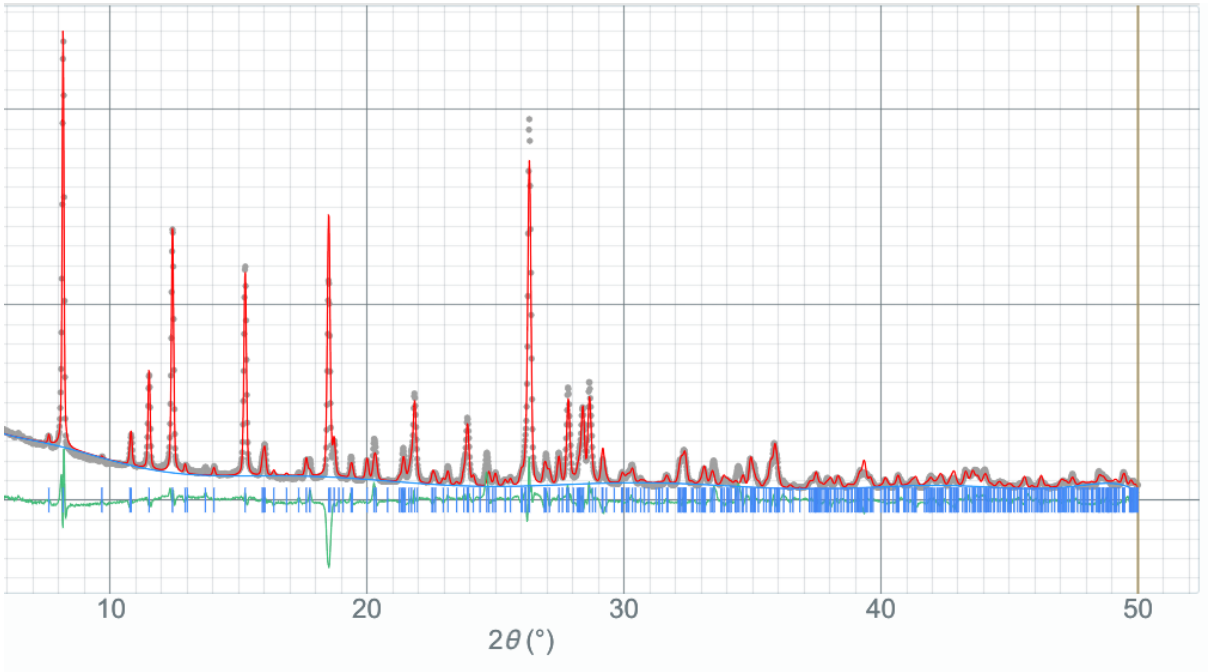

(b)

Fig. S32. (a) Experimental PXRD pattern of compound **1** compared with the simulated pattern from single-crystal X-ray diffraction. (b) Rietveld refinement plot of **1** using the single-crystal structure as the starting model. Observed intensities are shown as grey symbols, the calculated pattern as red solid line, and the difference curve (I_{obs} - I_{calc}) is shown at the bottom as green line. Vertical tick marks represent the Bragg positions.

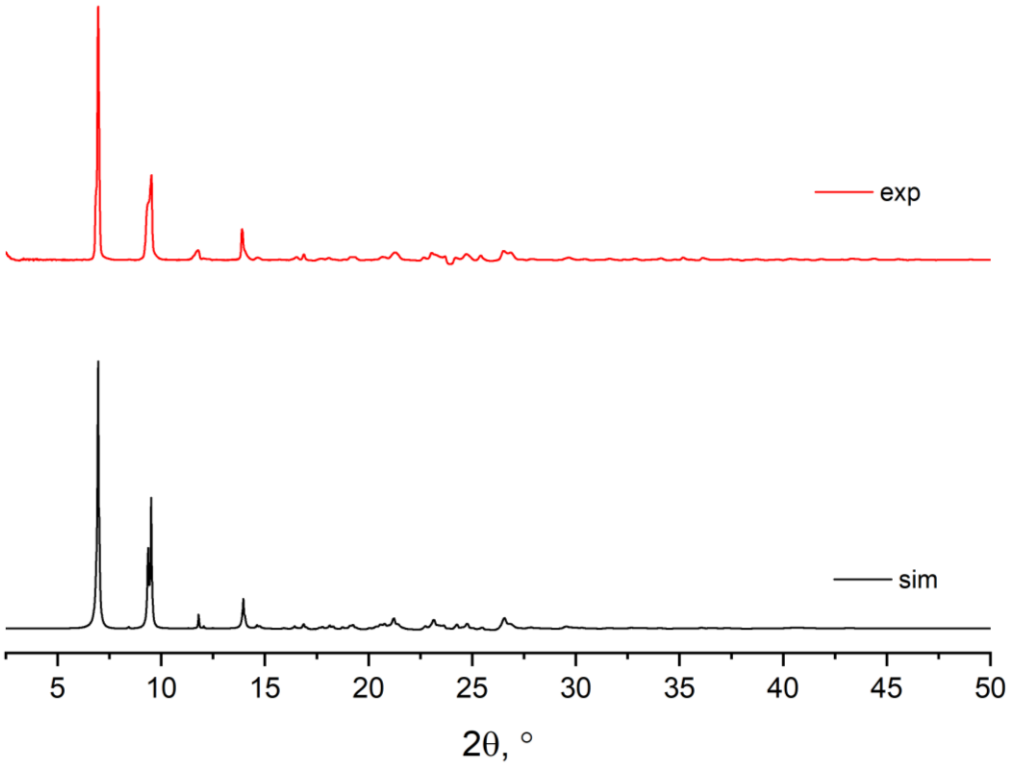

(a)

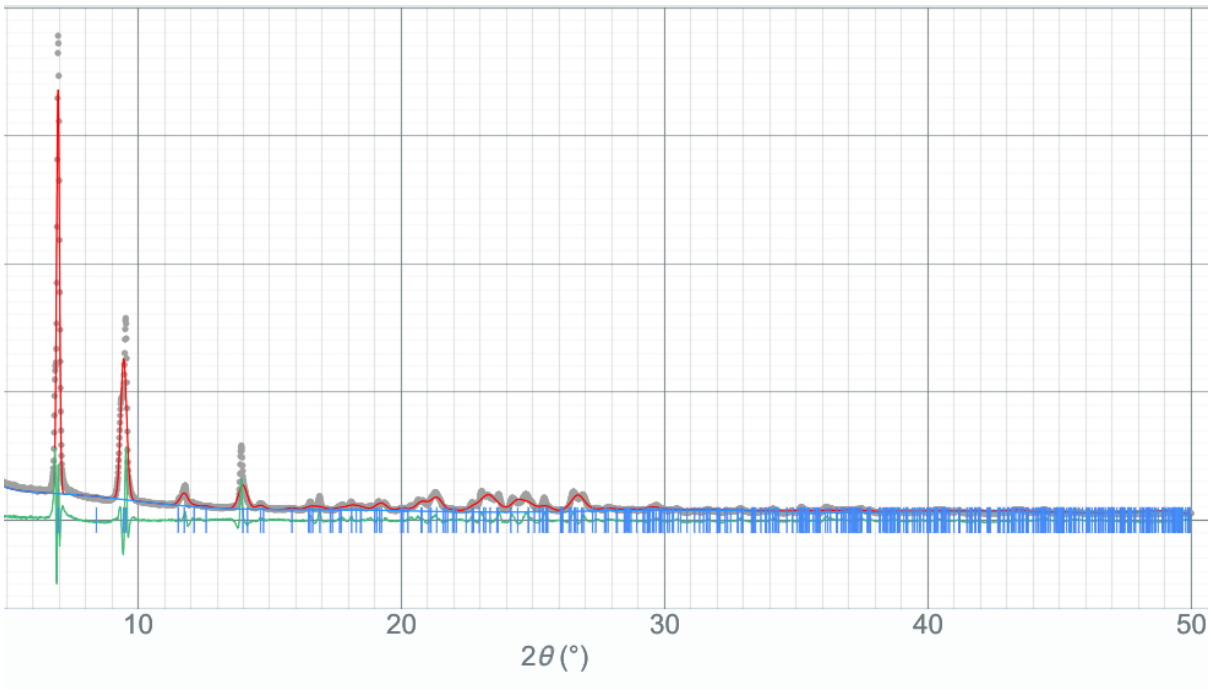

(b)

Fig. S33. (a) Experimental PXRD pattern of compound **2** compared with the simulated pattern from single-crystal X-ray diffraction. (b) Rietveld refinement plot of **2** using the single-crystal structure as the starting model. Observed intensities are shown as grey symbols, the calculated pattern as red solid line, and the difference curve (I_{obs} - I_{calc}) is shown at the bottom as green line. Vertical tick marks represent the Bragg positions.

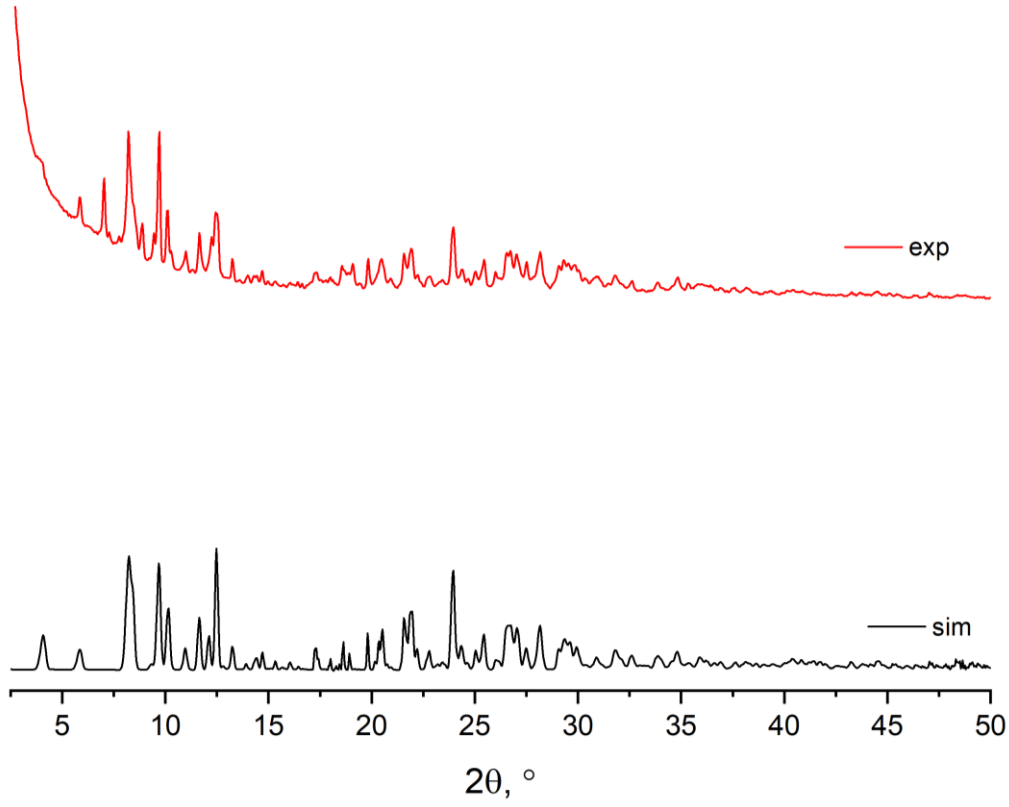

(a)

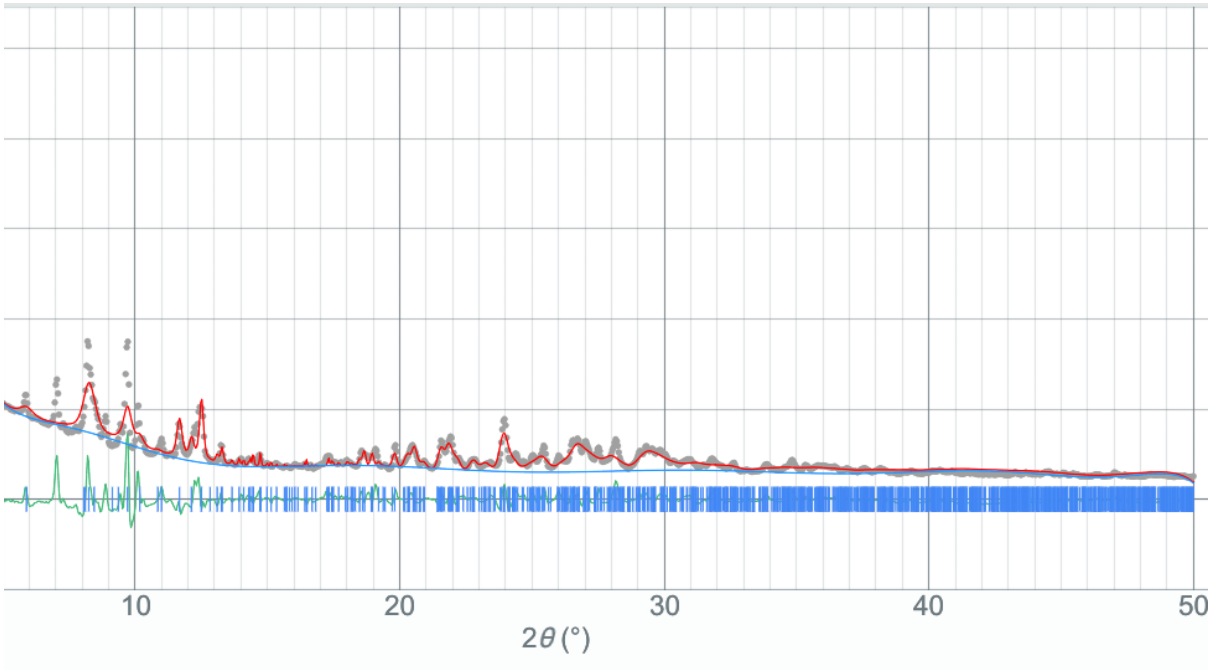

(b)

Fig. S34. (a) Experimental PXRD pattern of compound **3** compared with the simulated pattern from single-crystal X-ray diffraction. (b) Rietveld refinement plot of **3** using the single-crystal structure as the starting model. Observed intensities are shown as grey symbols, the calculated pattern as red solid line, and the difference curve (I_{obs} - I_{calc}) is shown at the bottom as green line. Vertical tick marks represent the Bragg positions.

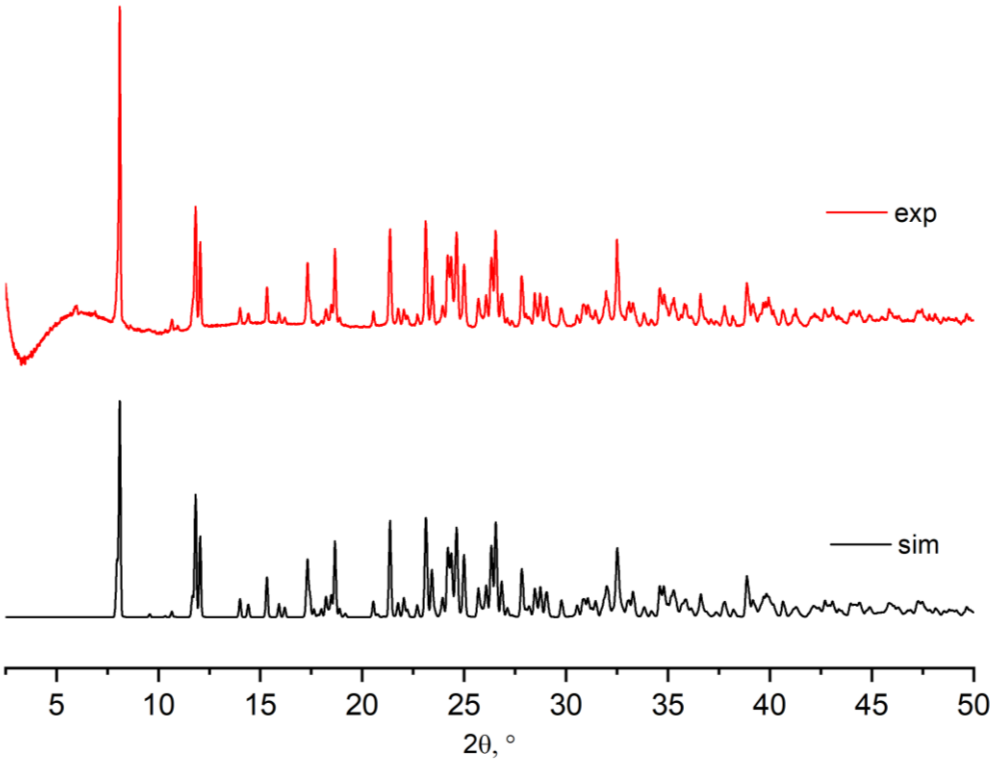

(a)

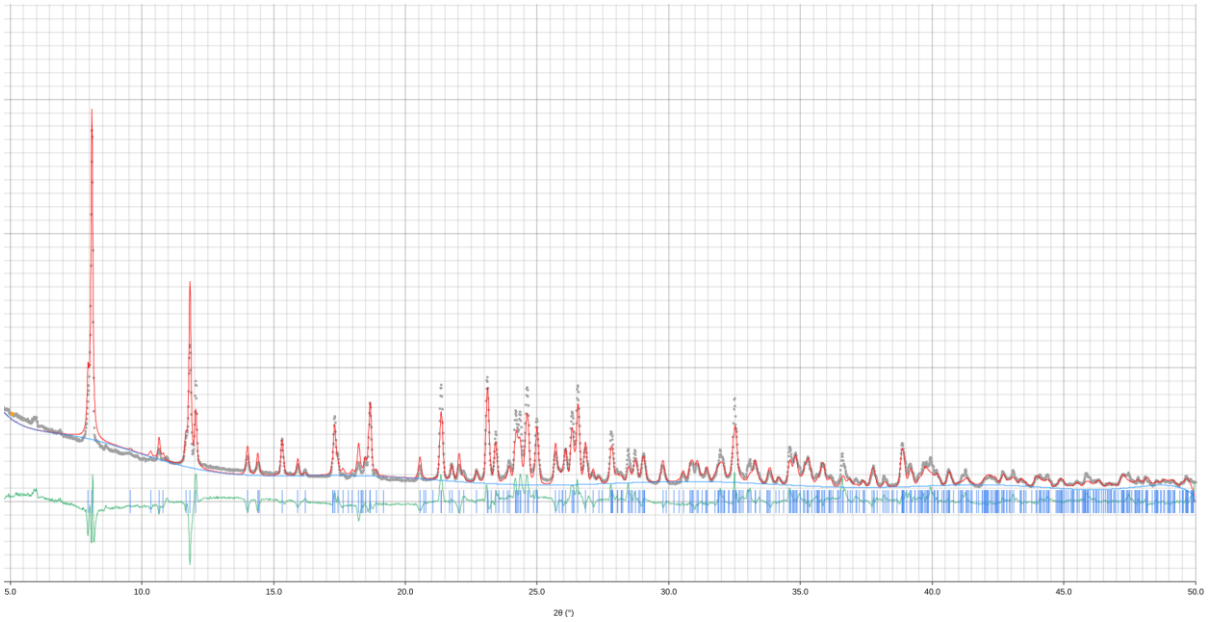

(b)

Fig. S35. (a) Experimental PXRD pattern of compound **4** compared with the simulated pattern from single-crystal X-ray diffraction. (b) Rietveld refinement plot of **4** using the single-crystal structure as the starting model. Observed intensities are shown as grey symbols, the calculated pattern as red solid line, and the difference curve (I_{obs} - I_{calc}) is shown at the bottom as green line. Vertical tick marks represent the Bragg positions.

Table S1. Crystal data and details of structural determinations for **1**-**4**

	1	**2**	**3**	**4**
Formula	$C_{17}H_{26}N_6O_{11}V_2$	$C_{42}H_{52}N_8O_{20}V_4$	$C_{34}H_{70.73}N_8Na_2O_{38.37}V_4$	$C_{17}H_{18}Cs_2N_4O_{11}V_2$
M_r/g mol^{-1}	592.32	1192.68	1455.33	821.29
T/K	293	100	200	200
Cryst. system	Triclinic	Monoclinic	Monoclinic	Monoclinic
Space group	P-1	$P2_1/c$	$P2_1/c$	$C2/c$
a/Å	9.4298(5)	12.6070(3)	22.3715(2)	16.2470(2)
b/Å	10.8957(6)	18.2159(4)	21.0369(2)	16.4323(2)
c/Å	11.9941(8)	10.6813(3)	13.4229(12)	19.9683(2)
α/°	85.710(5)	90	90	90
β/°	75.669(5)	93.299(2)	103.7215(9)	111.6234(12)
γ/°	86.699(4)	90	90	90
V/Å^3	1189.66(12)	2448.87(11)	6136.92(10)	4955.9(9)
Z	2	2	4	8
D_{calcd} / mg/m^3	1.653	1.617	1.575	2.201
μ / mm^{-1}	0.855	0.827	6.025	29.472
F(000)	608	1224	3007	
Crystal size / mm^3	0.20 x 0.05 x 0.05	0.20 x 0.05 x 0.03	0.10 x 0.05 x 0.05	0.18 x 0.15 x 0.05
Theta range for data collection / °	2.231 - 30.925	1.62 – 26.72	5.846 – 153.74	7.95 – 133.164
Index ranges	$-13 \le h \le 11$, $-14 \le k \le 14$, $-15 \le l \le 16$	$-15 \le h \le 14$, $-22 \le k \le 22$, $-13 \le l \le 12$	$-28 \le h \le 27$, $-25 \le k \le 25$, $-16 \le l \le 12$	$-19 \le h \le 17$, $-19 \le k \le 18$, $-23 \le l \le 23$
Refls collected/independent	17723/5998 (R_{int}=0.0382)	14830/4666 (R_{int}=0.0301)	49553/12155 (R_{int}=0.0325)	15673/4377 (R_{int}=0.0394)
Data/restrains/parameters	5998 /24/ 367	4666 / 0 / 342	12155 / 4 / 683	4377/1/332
Goodness-of-fit on F^2	1.095	1.05	1.084	1.030
Final R_1, wR_2	R_1=0.0377, wR_2 = 0.0980	R_1 = 0.0364, wR_2 = 0.087	R_1 = 0.0760, wR_2 = 0.2303	R_1 = 0.0332, wR_2 = 0.0906

R indices R_1, wR_2 (all data)	R_1 = 0.0532, wR_2 = 0.1042	R_1 = 0.0484, wR_2 = 0.0878	R_1 = 0.0850, wR_2 = 0.2399	R_1 = 0.0339, wR_2 = 0.0913
Largest diff. peak and hole / $e \cdot Å^{-3}$	0.363/ –0.32	0.483 / –0.312	1.93 / –0.74	1.20, –1.35
CCDC	2495523	2495524	2495525	2495527

Crystallographic measurements for **3** and **4** were carried out with a Rigaku XtaLAB Synergy Dualflex diffractometer with a HyPix detector using Cu Kα radiation at 200 K

Table S2. Selected bond distances (Å) in **1**–**4**

1							
V1−O1	1.9106(14)	V1−N1	2.1456(17)	V2−O5	1.9400(14)	V2−O7	1.6344(16)
V1−O2	1.6205(16)	V1−N3	2.0462(16)	V2−O6	1.6314(16)	V2−N4	2.1989(16)
V1−O3	1.6407(14)	V2−O4	1.8811(14)				
2							
V1−O1	1.8844(18)	V1−N1	2.168(2)	V2−O4	1.8281(17)	V2−O9	1.7619(17)
V1−O6	1.6305(17)	V1−N3	2.0858(19)	V2−O8	1.5903(18)	V2−N4	2.1694(19)
V1−O7	1.6211(17)	V2−O3	1.9833(16)				
3							
V1A−O2A	1.918(3)	V2A−O5A	1.963(3)	Na1A−O1A	2.441(3)	Na1B−O1WY	2.349(9)
V1A−O3A	1.646(3)	V2A−O6A	1.880(4)	Na1A−O1WA	2.309(7)	Na1B−O2B	2.353(4)
V1A−O4A	1.617(3)	V2A−O8A	1.625(4)	Na1A−O1WX	2.355(11)	Na1B−O2WB	2.409(6)
V1A−N1A	2.165(4)	V2A−O9A	1.650(4)	Na1A−O2A	2.355(3)	Na1B−O3B	2.923(4)
V1A−N3A	2.059(3)	V2A−N4A	2.173(4)	Na1A−O2WA	2.356(7)	Na1B−O6B^{2}	2.547(4)
V1B−O2B	1.911(3)	V2B−O5B	1.945(4)	Na1A−O2WX	2.381(8)	Na1B−O9B^{2}	2.441(5)
V1B−O3B	1.645(4)	V2B−O6B	1.881(4)	Na1A−O3A	2.874(3)	Na1B−O1WB	2.375(6)
V1B−O4B	1.623(4)	V2B−O8B	1.639(5)	Na1A−O6A^{1}	2.739(5)	^{1}-*x*,1-*y*,2-*z*;^{2}1-*x*,1-*y*,3-*z*	
V1B−N1B	2.171(4)	V2B−O9B	1.638(4)	Na1A−O9A^{1}	2.425(4)		
V1B−N3B	2.038(3)	V2B−N4B	2.170(4)	Na1B−O1B	2.438(4)		
4							
V1−O2	1.894(3)	Cs1X−O2W	3.188(8)	Cs1−O2W	2.993(2)	Cs2−O3^{5}	3.083(3)
V1−O3	1.654(3)	Cs1X−O2	3.162(5)	Cs1−O2	3.165(2)	Cs2−O4^{5}	3.121(3)
V1−O4	1.622(3)	Cs1X−O3WX	3.806(17)	Cs1−O3W	3.375(9)	Cs2−O4^{4}	3.140(3)
V1−O5	1.964(3)	Cs1X−O3	3.143(6)	Cs1−O3WX	3.352(11)	Cs2−O7^{4}	3.303(3)
V1−N1	2.165(3)	Cs1X−O6^{2}	3.185(7)	Cs1−O3WX^{1}	3.73(2)	Cs2−O7	3.132(3)

V2−O6	1.636(3)	Cs1X−O8[2]	3.192(8)	Cs1−O3	3.075(3)	Cs2−O8	3.120(3)
V2−O7	1.636(3)	Cs1X−O9[2]	2.880(13)	Cs1−O6[2]	3.043(3)	Cs2−O9	3.311(3)
V2−O8	1.903(3)	Cs1X−N3[3]	3.426(6)	Cs1−O8[2]	3.428(4)	[1]2-*x*,+*y*,3/2-*z*; [2]1/2+*x*,1/2-*y*,1/2+*z*; [3]3/2-*x*,-1/2+*y*,3/2-*z*; [4]1/2-*x*,1/2-*y*,1-*z*; [5]-1/2+*x*,1/2-*y*,-1/2+*z*	
V2−N2	2.027(3)	Cs1−O1	3.038(3)	Cs1−O9[2]	3.304(4)		
V2−N4	2.152(3)	Cs1−O1W	3.556(4)	Cs1−N3[3]	3.505(3)		

Table S3. Details of the hydrogen bonding interactions in **1**-**4**

Contact D–H···A	Distance, Å			Angle DHA, °	Symmetry transformations
	D–H	H···A	D···A		
1					
O10–H10A···O2	0.837(17)	2.32(2)	3.074(3)	149(3)	1–*x*,1–*y*,1–*z*
O10–H10B···O7	0.839(18)	2.22(2)	3.033(3)	163(3)	1–*x*, –*y*,1–*z*
O11–H11A···N2	0.836(17)	1.945(18)	2.777(2)	174(3)	*x*, *y*, *z*
O11–H11B···O2	0.824(17)	2.134(19)	2.944(2)	167(3)	1–*x*,1–*y*, –*z*
N5–H5A···O10	0.855(10)	1.989(12)	2.823(3)	166(3)	*x*, *y*, *z*
N5–H5B···O7	0.853(10)	2.238(11)	3.090(3)	176(3)	*x*, *y*, *z*
N5–H5C···O1	0.855(11)	2.28(2)	2.920(3)	132(2)	1–*x*,1–*y*,1–*z*
N5–H5C···O8	0.855(11)	2.136(17)	2.910(3)	150(3)	1–*x*,1–*y*,1–*z*
N5–H5D···O3	0.856(12)	2.048(12)	2.899(3)	172(3)	*x*, *y*, *z*
N6–H6A···O4	0.848(10)	2.166(16)	2.968(3)	158(3)	–1+*x*, *y*, *z*
N6–H6A···O9	0.848(10)	2.30(3)	2.919(3)	130(3)	–1+*x*, *y*, *z*
N6–H6B···O11	0.853(11)	1.992(11)	2.843(3)	175(3)	*x*, *y*, *z*
N6–H6C···O6	0.852(12)	2.093(19)	2.889(3)	155(4)	1–*x*, –*y*, –*z*
N6–H6B···O11	0.850(12)	2.40(3)	3.075(3)	137(3)	1–*x*, –*y*, –*z*
2					
N2–H2···O20	0.933	1.838	2.769(3)	175(2)	*x*, *y*, *z*
O20–H20···O7	0.84	2.08	2.912(2)	171(2)	–*x*,1/2+*y*,3/2–*z*
3					
O2W–H2WH···O5A	0.87	2.76	3.374(8)	129.4	–*x*, 1–*y*, 2–*z*
O1WA–H1WA··O1W	0.87	1.64	2.461(8)	155.9	*x*, *y*, *z*
O2WB–H2WE···O2WX	0.88	2.23	2.835(13)	125.8	*x*, *y*, 1+*z*
O2WX–H2WD···O7A	0.86	2.51	3.178(11)	136.0	–*x*, 1–*y*, 2–*z*
4					
O1W–H···O3	0.86	2.19	2.805(4)	127.4	*x*, *y*, *z*
O3W–H···O1W	0.83	2.38	2.812(8)	113.3	*x*, *y*, *z*
O3WX–H···O1W[1]	0.87	2.44	2.841(13)	143.8	*2-x,+y,3/2-z*
O3WX–H···O1W	0.88	2.35	2.85(2)	116.0	*x*, *y*, *z*

Table S4. Continuous shape measures (CShM) of the coordination geometries of V(V) centers in **1-4** using SHAPE v2.0 [1]*

		PP-5	*vOC-5*	*TBPY-5*	*SPY-5*	*JTBPY-5*
	ML5	Pentagon (D_{5h})	Vacant octahedron (C_{4v})	Trigonal bipyramid (D_{3h})	Spherical square pyramid (C_{4v})	Johnson trigonal bipyramid J12 (D_{3h})
1	V1	27.903	3.227	3.567	**1.859**	5.276
	V2	30.880	2.360	3.674	**1.105**	5.736
2	V1	27.460	5.099	**2.949**	3.661	4.630
	V2	28.364	**1.041**	7.053	1.704	7.833
3	V1A	27.838	2.854	3.973	**1.740**	5.636
	V2A	30.043	1.553	5.523	**0.924**	7.510
	V1B	28.007	2.507	4.388	**1.386**	6.181
	V2B	30.412	1.532	5.634	**0.809**	7.697
4	V1	30.301	1.607	5.340	**0.830**	7.367
	V2	28.342	5.684	**2.447**	4.123	4.241

∗A value of zero corresponds to an exact match of the corresponding center to the ideal geometry.

[1] (a) M. Llunell, D. Casanova, J. Cirera, P. Alemany, S. Alvarez, *SHAPE 2.0*, Universitat de Barcelona, Barcelona, **2010**; (b) S. Alvarez , P. Alemany, D. Casanova, J. Cirera, M. Llunell, D. Avnir, *Coord. Chem. Rev.* **2005**, *249*, 1693–1708.

Table S5. Continuous shape measures (CShM) of the coordination geometries of alkali metal centers in **3-4** using SHAPE v2.0 [1]*

		HP-7	*HPY-7*	*PBPY-7*	*COC-7*	*CTPR-7*	*JPBPY-7*	*JETRY-7*
	[ML7]	Heptagon (D_{7h})	Hexagonal pyramid (C_{6v})	Pentagonal pyramid (D_{5h})	Capped octahedron (C_{3v})	Capped trigonal prism (C_{2v})	Johnson pentagonal bipyramid J13 (D_{5h})	Johnson elongated triangular pyramid J7 (C_{3v})
3	Na1A	28.124	20.117	8.201	4.016	**3.286**	11.944	14.307
	Na1B	28.982	19.205	7.639	**3.015**	3.159	10.585	15.698
4	Cs2	27.082	13.706	24.121	19.459	18.288	24.467	**11.288**

		OP-8	*HPY-8*	*HBPY-8*	*CU-8*	*SAPR-8*	*TDD-8*	*JGBF-8*	*JETBPY-8*	*JBTPR-8*	*BTPR-8*	*JSD-8*	*TT-8*	*ETBPY-8*
	[ML8]	Octagon (D_{8h})	Heptagonal pyramid (C_{7v})	Hexagonal bipyramid (D_{6h})	Cube (O_h)	Square antiprism (D_{4d})	Triangular dodecahedron (D_{2d})	Johnson gyrobifastigium J26 (D_{2d})	Johnson elongated triangular bipyramid J14 (D_{3h})	Biaugmented trigonal prism J50 (C_{2v})	Biaugmented trigonal prism (C_{2v})	Snub diphenoid J84 (D_{2d})	Triakis tetrahedron (T_d)	Elongated trigonal bipyramid (D_{3h})
4	Cs1	23.763	19.297	16.351	17.870	17.808	17.667	14.716	20.023	14.878	14.183	17.038	17.355	**13.430**

		DP-10	*EPY-10*	*OBPY-10*	*PPR-10*	*PAPR-10*	*JBCCU-10*	*JBCSAP-10*	*JMBIC-10*	*JATDI-10*	*JSPC-10*	*SDD-10*	*TD-10*	*HD-10*

	[ML10]	Decagon (D_{10h})	Enneagonal pyramid (C_{9v})	Octagonal bipyramid (D_{8h})	Pentagonal prism (D_{5h})	Pentagonal antiprism (D_{5d})	Bicapped cube J15 (D_{4h})	Bicapped square antiprism J17 (D_{4d})	Metabidiminished icosahedron J62 (C_{2v})	Augmented tridiminished icosahedron J64 (C_{3v})	Sphenocorona J87 (C_{2v})	Staggered Dodecahedron (2:6:2) (D_2)	Tetradecahedron (2:6:2) (C_{2v})	Hexadecahedron (2:6:2) or (1:4:4:1) (D_{4h})
4	Cs1	36.422	25.713	16.442	**9.163**	15.001	15.066	14.063	9.572	10.519	10.815	10.780	9.830	12.211

∗A value of zero corresponds to an exact match of the corresponding center to the ideal geometry.

[1] (a) M. Llunell, D. Casanova, J. Cirera, P. Alemany, S. Alvarez, *SHAPE 2.0*, Universitat de Barcelona, Barcelona, **2010**; (b) S. Alvarez , P. Alemany, D. Casanova, J. Cirera, M. Llunell, D. Avnir, *Coord. Chem. Rev.* **2005**, *249*, 1693–1708.